

1 **Regional and seasonal radiative forcing by perturbations to**
2 **aerosol and ozone precursor emissions**

3 **Nicolas Bellouin¹, Laura Baker¹, Øivind Hodnebrog², Dirk Olivié³, Ribu**
4 **Cherian⁴, Claire Macintosh¹, Bjørn Samset², Anna Esteve^{1,*}, Borgar Aamaas²,**
5 **Johannes Quaas⁴, and Gunnar Myhre².**

6 [1]{Department of Meteorology, University of Reading, Reading, United Kingdom}

7 [2]{Center for International Climate and Environmental Research – Oslo (CICERO), Oslo,
8 Norway}

9 [3]{Norwegian Meteorological Institute, Oslo, Norway}

10 [4]{Universität Leipzig, Leipzig, Germany}

11 [*]{now at: University of Valencia, Valencia, Spain}

12 Correspondence to: N. Bellouin (n.bellouin@reading.ac.uk)

13

1 **Abstract**

2- Predictions of temperature and precipitation responses to changes in the anthropogenic
3 emissions of climate forcers require the quantification of the radiative forcing exerted by
4 those changes. This task is particularly difficult for near-term climate forcers like aerosols,
5 methane, and ozone precursors because their short atmospheric lifetimes cause regionally and
6 temporally inhomogeneous radiative forcings. This study quantifies specific radiative forcing,
7 defined as the radiative forcing per unit change in mass emitted, for eight near-term climate
8 forcers as a function of their source regions and the season of emission by using dedicated
9 simulations by four general circulation and chemistry-transport models. Although differences
10 in the representation of atmospheric chemistry and radiative processes in different models
11 impede the creation of a uniform dataset, four distinct findings can be highlighted. Firstly,
12 specific radiative forcing for sulphur dioxide and organic carbon are stronger when aerosol-
13 cloud interactions are taken into account. Secondly, there is a lack of agreement on the sign of
14 the specific radiative forcing of volatile organic compound perturbations, suggesting they are
15 better avoided in climate mitigation strategies. Thirdly, the strong seasonalities of the specific
16 radiative forcing of most forcers allow strategies to minimise positive radiative forcing based
17 on the timing of emissions. Finally, European and shipping emissions exert stronger aerosol
18 specific radiative forcings compared to East Asia where the baseline is more polluted. This
19 study can therefore form the basis for further refining climate mitigation options based on
20 regional and seasonal controls on emissions. For example, reducing summertime emissions of
21 black carbon and wintertime emissions of sulphur dioxide in the more polluted regions is a
22 possible way to improve air quality without weakening the negative radiative forcing of
23 aerosols.

24

25 Keywords: Radiative forcing; near-term climate forcers; Aerosols; Methane; Ozone

26

1 **1 Introduction**

2 Human activities have profoundly modified the composition of the atmosphere by increasing
3 the concentrations of long-lived greenhouse gases, such as carbon dioxide or
4 chlorofluorocarbons, and medium- to short-lived species, such as methane (CH₄),
5 tropospheric ozone and aerosols. Once in the atmosphere, those species perturb the energy
6 budget of the Earth, exerting a radiative forcing (RF) of the climate system by various
7 mechanisms, namely greenhouse gas and ozone absorption of longwave radiation, and ozone
8 absorption and aerosol-radiation interactions (here denoted as following Boucher et al., 2013)
9 in the shortwave spectrum. Changes in aerosol concentrations also translate in aerosol-cloud
10 interactions (aci) through changes in the number of cloud condensation nuclei, modifying the
11 radiative properties and life cycle of clouds. In addition, aerosols that absorb shortwave
12 radiation, such as mineral dust and black carbon aerosols, change the surface albedo when
13 depositing on snow or ice. The tight interactions between gaseous and aerosol species add
14 components to the RF caused by complex feedbacks of one species onto another (von
15 Schneidmesser et al., 2015; Fiore et al., 2015). For example, changes in methane
16 concentrations trigger changes in tropospheric ozone, which exert primary-mode ozone RF
17 (Prather, 1996). Moreover, the hydroxyl radical OH links the atmospheric chemistry of ozone
18 and the oxidation of aerosol gaseous precursors, and Shindell et al. (2009) found sizeable
19 impacts of nitrogen oxides (NO_x), carbon monoxide (CO), and CH₄ emissions on aerosol
20 formation in global simulations of atmospheric chemistry.

21 There is also complexity in the concept of RF. In its traditional definition of stratospherically-
22 adjusted RF, surface and tropospheric conditions are held fixed to their unperturbed state, but
23 stratospheric temperatures are allowed to adjust. The fifth assessment report of the
24 Intergovernmental Panel on Climate Change (IPCC) has recently formalised a new definition,
25 called effective RF (ERF; Boucher et al., 2013; Myhre et al., 2013a), which also includes
26 rapid adjustments to the tropospheric state. Those rapid adjustments occur on shorter
27 timescales than deep ocean and sea ice changes and include such processes as the change in
28 cloud cover that follows the local atmospheric warming caused by aerosol absorption of
29 shortwave radiation, the change in cloud cover due to aerosol-driven changes in precipitation
30 efficiency, the increased spring melting that follows black carbon deposition on snow, or the
31 change in cloud cover that immediately follows changes in thermodynamic profiles in

1 response to an increase in carbon dioxide concentrations. Because ERF includes rapid
2 adjustments, it is a better indicator of the eventual surface temperature response than RF,
3 although an additional efficacy may be needed to account for the ability of ERF patterns
4 predominantly located in the Northern Hemisphere to cause more rapid land surface
5 temperature responses (Shindell, 2014). Both stratospherically-adjusted and effective RF
6 exclude the radiative impact of large-scale changes in sea surface temperatures, which are part
7 of the climate response.

8 Climate change mitigation options aim to eventually reduce and suppress the positive
9 industrial-era ERF currently exerted on the Earth's energy budget by human activities.
10 A difficulty in that task is that the basket of species emitted by a given sector of activity
11 changes in response to policies and technological advances (e.g. Smith et al., 2013). To
12 compare the climate impact of the emissions of different species while allowing for changes
13 in their emission rates, one therefore requires the knowledge of the RF exerted per change in
14 unit mass emission rate, hereafter called specific RF (SRF) and given in $\text{mW m}^{-2} (\text{Tg yr}^{-1})^{-1}$.
15 Combining the SRF of a species with its lifetime produces such climate metrics as the Global
16 Warming Potential or the Global Temperature Change Potential (e.g. Shine et al., 2005). In
17 the past, the available literature has been used in a rather ad-hoc way to quantify SRF. Table 1
18 summarises estimates from five previous multi-model studies. Bond et al. (2013), Myhre et al.
19 (2013b), Shindell et al. (2013) and Stevenson et al. (2013) estimate SRF for industrial-era
20 global emission changes. The SRFs from Fry et al. (2012) and Yu et al. (2013) are based on
21 20% reductions in the emissions of four regions. Table 1 also shows results for the present
22 study to allow for an easy comparison: those results are discussed in Sect. 4.

23 All studies agree on the sign of the SRF of individual species. Black carbon (BC) aerosols,
24 methane, CO and volatile organic compounds (VOCs) exert positive SRFs, which lead to a
25 gain in energy for the climate system when emissions are increased. In contrast, sulphate,
26 organic carbon (OC), and nitrate aerosols, and nitrogen oxides (NO_x), exert negative SRFs.
27 According to those studies, BC exerts the strongest SRF of all near-term climate forcers
28 (NTCFs), in absolute values. Its SRF is an order of magnitude larger than that of the other
29 aerosol species. The SRF of nitrogen oxides is the strongest of the ozone precursors, being for
30 example about 16 times larger than and of opposite sign to CO SRF. The strength of the SRF
31 of a given NTCF is however only one aspect of its climate impact: the strength of

1 anthropogenic emission rates also matters. Therefore, the strong SRFs of BC and NO_x have to
2 be considered in the context of their small emission rates relative to other precursors like
3 sulphur dioxide (SO₂) and CO. Regionally for ozone precursor perturbations, Fry et al. (2012)
4 find that South Asia exerts the strongest SRF for NO_x and VOC perturbations, while CO
5 perturbations exhibit little regional dependence. Aerosol contributions to net ozone precursor
6 SRFs vary in both sign and magnitude among models, and also regionally. For aerosol
7 perturbations, Yu et al. (2013) find that East Asian SO₂ emissions exert an SRF that is only
8 75% of that by European emissions, a smaller value attributed to a limitation in sulphur-cycle
9 oxidants over East Asia, which suppresses conversion of SO₂ to sulphate aerosols in that
10 region. Furthermore, their estimate of BC SRF from European emissions is 30% stronger than
11 that of other regions, a result attributed to the geographical extent of European aerosol
12 transport, which covers in particular the bright surfaces of the Arctic and Sahara, where BC
13 aerosols exert a strong positive RF.

14 The five studies listed in Table 1 report a sizeable amount of diversity in SRF estimates
15 among models. That diversity reflects different aerosol optical properties (Myhre et al.,
16 2013b) and vertical distributions (Samset et al., 2013), differences in cloud distributions,
17 surface properties, and radiative transfer (Stier et al., 2013; Randles et al., 2013; Stevenson et
18 al., 2013), large differences in the parameterised sensitivity of cloud albedo to aerosol
19 changes (Quaas et al., 2009), and differences in unperturbed ozone and aerosol levels
20 (Stevenson et al., 2013; Carslaw et al., 2013). Faced with model diversity, Myhre et al.
21 (2013b) choose to include all models in their best estimates while Shindell et al. (2013)
22 choose to select the models best able to represent present-day aerosol distributions and recent
23 trends. Bond et al. (2013) scale modelled RF towards stronger values mainly through
24 increases in emissions to account for a perceived low bias in simulated BC concentrations and
25 absorption aerosol optical depth. This upward scaling has been challenged by recent studies,
26 which reduce the BC underestimation in their models by instead improving the model
27 horizontal resolution (Wang et al., 2014a) or reducing BC lifetime (Samset et al., 2014).
28 Taken together, the variable experimental designs of multi-model studies and different
29 choices made to account for diversity hinder a clean assessment of the metrics uncertainty
30 caused by diversity in RF estimates (Fuglestad et al., 2010).

1 In addition, several policy choices are not addressed by existing studies. First, they do not
2 include all radiative forcing mechanisms consistently. RFaci and contributions to BC RF from
3 deposition on snow and rapid adjustments from the semi-direct effect are often excluded.
4 Then, although it is clearly important to take a regional view like that of Fry et al. (2012) and
5 Yu et al. (2013), it is potentially equally important to account for the seasonality of the
6 emissions. RF mechanisms based on perturbations of sunlight are obviously strongly
7 seasonal, so it is misleading to use year-long perturbations to quantify mitigation options that
8 mostly act, because of the short lifetimes of NTCFs, for wintertime (e.g. domestic heating) or
9 summertime (e.g. air conditioning) periods.

10 To remove those limitations, the Evaluating the CLimate and Air Quality ImPacts of Short-
11 livEd Pollutants (ECLIPSE) project (Stohl et al., 2015) built a matrix of SRFs that includes
12 several NTCFs, varies the region and time of emissions, and spans diversity among models.
13 This study documents that matrix while providing potential solutions for reducing model
14 diversity. SRFs are calculated for reductions in the anthropogenic emissions of primary
15 aerosols (BC, OC), aerosol precursors (sulphur dioxide, ammonia), ozone and secondary
16 aerosol precursors (NO_x, CO, VOC), and methane. The regional view comes from focusing
17 on two source regions, Europe and East Asia, and singling out the shipping sector. Emissions
18 are perturbed seasonally, to assess which of local summer or wintertime emission reductions
19 are most effective at exerting an SRF. Most radiative mechanisms are also quantified: RFaci
20 is systematically included, ozone precursor RFs include a contribution from aerosol changes
21 that arise through aerosol-chemistry couplings, and contributions to BC RF from deposition
22 on snow and rapid adjustments from the semi-direct effect are also estimated, albeit from a
23 single model. This study neglects the very weak ozone and methane RF exerted by
24 perturbations of aerosol primary or precursor emissions through changes in OH distributions.

25 The paper is structured as follows. Section 2 describes the participating models and
26 experimental design. Section 3 quantifies the components of SRF simulated by each model as
27 a function of emitted species, region, and season. Causes of model diversity are also identified
28 and discussed. Section 4 gives the best estimate of the SRF matrix resulting from the
29 ECLIPSE project. Finally, Sect. 5 concludes with a discussion of research priorities for
30 decreasing model diversity, recommendations for climate mitigation options, and possible

1 solutions to the difficulties encountered when quantifying rapid adjustments. Supplementary
2 Figures show annually-averaged distributions of RF components for all perturbations.

3

4 **2 Models and experimental protocol**

5 Participating models are ECHAM6-HAM2, HadGEM3-GLOMAP, NorESM1, and
6 OsloCTM2. It is known from previous participations of those models in multi-model inter-
7 comparisons (Myhre et al., 2013b, Stevenson et al., 2013, Shindell et al., 2013) that those four
8 models span a large range of inter-model diversity for both aerosol and ozone. Models differ
9 in horizontal and vertical resolution and in the number of aerosol species included (Table 2).
10 In particular, OsloCTM2 is the only model that represents nitrate aerosols. ECHAM6 does not
11 simulate secondary organic aerosols, and also lacks interactive ozone chemistry, and thus did
12 not perform perturbations to ozone precursor emissions.

13 ECHAM6-HAM2 is the European Centre for Medium-Range Weather Forecasts (ECMWF)
14 Hamburg model version 6 (Stevens et al., 2013). Its radiation scheme is RRTM-G (Iacono et
15 al., 2008). Aerosols are represented by the two-moment Hamburg Aerosol Model (HAM)
16 version 2 (Zhang et al., 2012), which consists of the microphysical module M7 that simulates
17 seven internally-mixed aerosol modes (Vignati et al., 2004; Stier et al., 2005). Aerosol
18 interactions with liquid and frozen water clouds follow Lohmann et al. (2007).

19 HadGEM3 is the Hadley Centre Global Environment Model version 3 (Hewitt et al., 2011).
20 Its radiation scheme is described by Edwards and Slingo (1996). Gas-phase chemistry is
21 modelled by the United Kingdom Chemistry and Aerosols (UKCA) TropIsop scheme, which
22 treats 55 chemical species (37 of which being transported) including hydrocarbons and
23 isoprene and its degradation products (O'Connor et al., 2014). Aerosols are coupled to the
24 chemistry, and modelled by UKCA-GLOMAP (GLobal Model of Aerosol Processes, Mann et
25 al., 2010), which represents the size-resolved internal mixture using a two-moment modal
26 approach and four soluble and insoluble aerosol modes. Aerosols interact with liquid clouds
27 only, following the empirical relationship between aerosol number and cloud droplet number
28 concentration established by Jones et al. (1994).

29 NorESM1-M is the Norwegian Earth System Model version 1 (Bentsen et al., 2013; Iversen et
30 al., 2013). Its atmosphere and aerosol module is CAM4-Oslo (Kirkevåg et al., 2013) and the

1 radiation scheme is described by Collins (2001). In the version used in this study, aerosols
2 (described by 20 tracers) are fully coupled to the MOZART tropospheric gas-phase chemistry
3 scheme (Emmons et al., 2010), which treats 84 gaseous species. Aerosol mass concentrations
4 are simulated in four size classes: nucleation, Aitken, accumulation, and coarse modes.

5 OsloCTM2 is the CTM of the University of Oslo and the Center for International Climate and
6 Environmental Research – Oslo (CICERO) (Myhre et al., 2009; Skeie et al., 2011). The
7 model is driven by meteorological data generated by the Integrated Forecast System (IFS)
8 model at ECMWF. The model simulates the tropospheric chemistry of 67 species (Dalsøren et
9 al., 2007). Aerosols are simulated as external mixtures of 7 aerosol types, including nitrate, as
10 described by Skeie et al. (2011). RFari and RFaci are computed by offline radiative transfer
11 calculations, as described in Myhre et al. (2007) and Skeie et al. (2011). Myhre et al. (2000)
12 describes the offline calculations performed to obtain ozone radiative forcing.

13 The 48 ECLIPSE RF simulations are listed in Table 3. Simulations are free-running with
14 fixed sea-surface temperature and sea-ice distributions. Simulations last only 1 year after
15 spin-up because RF by definition excludes changes in the tropospheric state so inter-annual
16 differences in meteorology are the only source of variability between simulations.
17 Meteorology affects transport and removal processes, especially wet deposition, and to a
18 lesser extent chemical production when driven by temperature or availability of sunlight.
19 Perturbation simulations made with HadGEM3 were extended to 3 years and suggest that
20 inter-annual variability never exceeds $\pm 10\%$ of globally-averaged RF, which is small
21 compared to inter-model diversity.

22 Control emissions are taken from the ECLIPSE dataset version 4a (Stohl et al., 2015;
23 <http://www.iiasa.ac.at/web/home/research/researchPrograms/air/ECLIPSEv4a.html>) for the
24 year 2008. A seasonal cycle has been applied to the emissions of the domestic sector, to
25 reflect changes in domestic heating as a function of temperature. This seasonal cycle is
26 obtained by multiplying annual total domestic sector emissions by a gridded dataset of
27 monthly weights, obtained by the Mitigation of Arctic warming by Controlling European
28 Black carbon emissions (MACEB) project following Sect. 3.3 of Streets et al. (2003), where
29 stove operation times are expressed as a function of climatological monthly-mean
30 temperature.

1 Emission perturbations involve a 20% decrease of primary and precursor emissions of the
2 given species in one of the following regions: Europe, East Asia, shipping, and Rest of the
3 World (RotW). Results for RotW are not presented directly in this paper: instead, global
4 results are given by adding Europe, East Asia, and RotW together. Applying a decrease,
5 rather than an increase, has been chosen because it better represents scientific
6 recommendations to air quality and climate policy (Schmale et al., 2014). The value of 20%
7 was chosen to be representative of typical technologically feasible emission reductions. The
8 same value was also used in previous HTAP simulations (Fry et al., 2012; Yu et al., 2013).
9 The definition of regions follows tier-1 HTAP regions (Figure 1). Here, Europe includes
10 European Union and European Economic Area countries, and Switzerland, Turkey, and
11 former Yugoslavia. East Asia includes China, Japan, Taiwan, North and South Korea, and
12 Mongolia. Because of the specific impact of the shipping sector on air quality (Viana et al.,
13 2014), its emissions have been perturbed independently, with all species emitted by that
14 sector being perturbed together, although OsloCTM2 and NorESM1 have run perturbations
15 for each species within the shipping sector (results not shown). Shipping emissions are taken
16 from the RCP6.0 dataset (Fujino et al., 2006) prepared for phase 5 of the Climate Model
17 Inter-comparison project (CMIP5), interpolated to 2008 between 2005 and 2010. All
18 perturbations are applied either in Northern Hemisphere summer (May-October) or winter
19 (November-April). The size of the emission perturbations is given in Table 3 and in Table 4
20 for shipping sector perturbations. The size of shipping emission perturbations is different for
21 ECHAM6-HAM, because RCP8.5 (Riahi et al., 2007) was used, and for NO_x in NorESM1,
22 because of a mistake when processing that particular dataset. The size of non-methane VOC
23 emission perturbations is model-dependent because the list of species emitted under the VOC
24 label depends on the model used: 5 for HadGEM3, 14 for NorESM1, and 12 for OsloCTM2.
25 As discussed in Sect. 3.3, differences in the VOC species included in the models add to SRF
26 diversity. For OsloCTM2, VOC emissions were converted to unit mass of carbon by
27 assuming a mean VOC atomic weight of 47 u.

28 Methane perturbations are achieved by scaling the prescribed concentrations or mass-mixing
29 ratios, rather than by perturbing emissions like for the other NTCFs. This difference in
30 treatment arises because HadGEM3, NorESM1, and OsloCTM2 prescribe global-mean
31 methane concentrations at the surface and then let the chemistry scheme determine the

1 vertical distribution, thus avoiding long spin-ups caused by the 12-year lifetime of methane in
2 the atmosphere. Scaled methane surface concentrations C are given by the equation:

$$3 \quad C = C_0 \cdot (E/E_0)^f \quad (\text{Eq. 1})$$

4 where C_0 are the control surface concentrations, E is the global emission rate where the
5 anthropogenic contribution has been reduced by 20%, and E_0 is the control global emission
6 rate. E/E_0 is therefore equal to 0.8 in this study. f is the feedback factor of methane on its own
7 lifetime, defined as the ratio of methane perturbation lifetime to total budget lifetime. The
8 value of f for each participating model was not known when preparing the simulations, and
9 was therefore taken at 1.34 following Holmes et al. (2013). As discussed in Sect. 3.2, actual
10 values of f range from 1.28 to 1.46, in reasonable agreement with the value initially assumed.
11 Because the long atmospheric lifetime of methane allows it to be well mixed geographically,
12 methane perturbations are not applied regionally. NorESM1 applied perturbations seasonally
13 (May—Oct and Nov—Apr) and found differences in SRF of only 7% between the two
14 seasons. Because that seasonal dependence is small, OsloCTM2 and HadGEM3 have applied
15 the perturbation for the whole year.

16 RF is calculated at the top of the atmosphere as the difference in net shortwave and longwave
17 radiative fluxes between the perturbed and control simulations. More specifically, three
18 methods are used to obtain stratospherically-adjusted RF from the perturbation simulations,
19 depending on the species being considered and whether the model is capable of interactive
20 radiation calculations (Table 1).

- 21 • To obtain the RF of aerosol perturbations in general circulation models, the model
22 evolution (its “meteorology”) is set to be independent of the perturbation. The method
23 used to achieve this independence involves diagnosing radiative fluxes with and without
24 the perturbation to the forcing agent included, with the second set of radiative fluxes used
25 to advance the model into its next time step. Stratospheric adjustment is neglected for
26 aerosols, because tropospheric aerosol perturbations have little effect on stratospheric
27 temperatures. Aerosol RF includes both ari and aci, except for ECHAM6, which only
28 diagnosed ari.
- 29 • To obtain the RF of aerosol perturbations in chemistry-transport models and the RF of
30 ozone exerted by ozone-precursor perturbations in all models, instantaneous RF is
31 computed by offline radiative transfer codes, using aerosol and trace gas distributions

1 obtained from the perturbation simulations. HadGEM3 ozone RF is computed with the
2 offline version of the radiative transfer code by Edwards and Slingo (1996). OsloCTM2
3 aerosol and ozone RF, and NorESM1 ozone RF, are computed with offline longwave and
4 shortwave radiative transfer codes as described in Myhre et al. (2000), Myhre et al.
5 (2007) and Skeie et al. (2011). For all models, ozone RF is adjusted for changes in
6 stratospheric temperatures.

- 7 • The RF of methane is computed using the analytical expression established by Myhre et
8 al. (1998), which accounts for stratospheric adjustments. Details of this calculation are
9 given in Sect. 3.2 below.

10 The four models simulate different aerosol and tropospheric ozone lifetimes, as shown in
11 Table 5. Sulphate and BC aerosol lifetimes vary by a factor 1.5. Modelled OC lifetime has a
12 larger diversity, with variations by a factor 2.5. Tropospheric ozone lifetime is also diverse:
13 HadGEM3 and NorESM1 disagree by a factor 1.3. OsloCTM2 did not diagnose it.
14 Differences in simulated lifetimes are thought to arise from virtually all aspects of the models,
15 including differences in the simulated present-day climate, the treatment of atmospheric
16 horizontal and vertical transport, atmospheric chemistry, and wet and dry deposition
17 processes. Large model spreads have long been a characteristics of aerosol and chemistry
18 inter-comparisons (e.g. Myhre et al., 2013b; Stevenson et al., 2013), in part because of a lack
19 of strong observational constraints on atmospheric lifetimes on a global scale (Kristiansen et
20 al., 2012; Hodnebrog et al., 2014). The four ECLIPSE models are representative of those
21 spreads.

22 Aerosol and ozone distributions simulated by the four models participating in this study have
23 been compared to observations as part of their development cycles (Bellouin et al., 2011;
24 Kirkevåg et al., 2013; O'Connor et al., 2014; Skeie et al., 2011; Zhang et al., 2012), multi-
25 model inter-comparisons (Koffi et al., 2016; Pan et al., 2015; Stevenson et al., 2013;
26 Tsigaridis et al., 2014), and within the ECLIPSE project (Eckhardt et al., 2015; Quennehen et
27 al., 2016; Schulz et al. 2015). Those evaluations draw a complex picture, where model skill at
28 reproducing NTCF distributions with fidelity differs among models and strongly depends on
29 region and species. Quennehen et al. (2016) compared the four ECLIPSE models to MODIS
30 (Moderate Resolution Imaging Spectroradiometer) aerosol optical depth (AOD) retrievals and
31 Cloud-Aerosol Lidar with Orthogonal Polarization (CALIOP) scattering profiles, finding

1 qualitative agreement but quantitative discrepancies that depend on model, season, and
2 region. The models tend to put aerosol scattering too high in the atmosphere, hinting that
3 transport into the free troposphere is too efficient or sinks are too weak. Such errors in
4 simulated vertical profiles may lead to too weak an SRF_{aci}, because aerosols end up being
5 simulated above clouds instead of interacting with them. For BC, placing the aerosols too
6 high in the atmosphere leads to overestimating R_{Fari} (Samset et al., 2013) and
7 underestimating rapid adjustments from semi-direct effects, so the net impact on SRF depends
8 on the local balance between those two mechanisms.

9 Evaluations of surface and total-column ozone (Schulz et al., 2015; Quennehen et al., 2016;
10 O'Connor et al., 2014) find that OsloCTM2 does the best simulation, both in terms of
11 magnitude and seasonality. HadGEM3 and NorESM1 tend to overestimate both surface
12 concentrations and the ozone column. The three models locate ozone too low in the
13 troposphere, but are still able to qualitatively reproduce the gradients existing between surface
14 concentrations in urban and rural conditions. However modelled gradients are smoothed out
15 because of the relatively coarse resolutions of the models.

16 RF and SRF cannot be evaluated against observations, so the challenge is to interpret what
17 regional evaluations of surface concentrations, vertical profiles and optical properties imply
18 for globally-averaged SRF to regional perturbations. Propagation of errors in the emission-
19 concentration-RF chain is often non-linear. Methane RF is proportional to the square root of
20 its concentration (Myhre et al., 1998). Ozone RF efficiency increases with altitude in the
21 troposphere with a maximum near the tropopause (Lacis et al., 1990) so ozone being located
22 too low in models introduces a low bias in the SRF exerted by ozone precursors. Aerosol RF
23 efficiency is affected by model failure to transport a NTCF to a region where surfaces are
24 highly reflective (deserts, ice, and snow) or the cloud regime is strongly susceptible to aerosol
25 influences (low maritime clouds). Locating BC aerosols too high up in the atmosphere so they
26 end up overlying bright clouds can overestimate their R_{Fari} efficiency by up to a factor of 2
27 (Hodnebrog et al., 2014). Aerosol-cloud interactions inherit the strong non-linearities between
28 aerosol and CCN concentrations (Hegg, 1994) and cloud droplet concentrations and cloud
29 albedo (Taylor and McHaffie, 1994) so biases in concentrations will have strong impacts on
30 RF estimates in regions where aerosol concentrations are small to moderate, away from
31 sources. The normalised nature of SRF and non-linearities in the emission-to-forcing chain

1 therefore preclude a simple scaling of modelled SRF with identified biases. This study
2 therefore reports SRF as simulated by the models but highlights in the next section the
3 implications of comparisons to observations for the SRF exerted by each species.

4

5 **3 Specific radiative forcing by species**

6 In this section, SRFs of aerosol, methane, ozone precursor, and shipping sector emission
7 perturbations are discussed in turn. SRF is stratospherically-adjusted but excludes rapid
8 adjustments in the troposphere, with one exception: rapid adjustments of BC semi-direct
9 effects have been computed independently and are discussed in Sect. 3.1. SRF is given for
10 May-October (hereafter labelled Summer for the sake of simplicity but also because emission
11 perturbations are disproportionately located in the Northern hemisphere) and November-April
12 (labelled Winter), for three regions (Europe, East Asia, and Global), and for the shipping
13 sector. Globally-averaged RF is computed as the sum of the European, East Asian, and RotW
14 perturbations. Although perturbations are not exactly additive, this is a good first-order
15 assumption.

16 **3.1 Aerosols and their precursors**

17 Figure 2 shows globally- and annually-averaged SRF for SO₂, BC, OC, and ammonia (NH₃)
18 perturbations in the ECLIPSE models. Ammonia perturbations have only been simulated by
19 OsloCTM2 because it is the only participating model that represents the equilibrium between
20 nitric acid, in the gas phase, and nitrate aerosols. ECHAM6 is consistently associated with
21 weaker SRF than other models because it only diagnoses ari, therefore neglecting the often
22 larger aci contribution – only for BC is aci a relatively minor component of aerosol RF, at 2 to
23 15% according to NorESM1 and OsloCTM2.

24 The SRF exerted by SO₂, OC, and NH₃ perturbations are negative. BC SRF is positive overall
25 because the positive contributions from ari and snow-albedo mechanisms are only partly
26 offset by negative contributions from aci and rapid adjustments from the semi-direct effect.
27 All models agree that aerosol SRF is stronger for Summer than Winter perturbations, which is
28 expected because RFari and RFaci act almost exclusively in the shortwave spectrum and are
29 therefore a strong function of solar irradiance. As shown in Figures S1 and S4, sulphate and

1 OC RF cover a larger area in models with longer sulphate and OC aerosol lifetimes (Table 5),
2 such as HadGEM3, than in models with shorter lifetimes, like OsloCTM2. This extended
3 coverage has two competing effects on the strength of SRF, both driven by non-linearities in
4 RFaci. On the one hand, a longer lifetime promotes stronger RFaci because emission
5 perturbations propagate more easily to remote regions where concentrations are low and
6 RFaci desaturates more easily. On the other hand, a longer lifetime weakens RFaci by
7 increasing concentrations in the reference simulation in those same remote regions, saturating
8 RFaci. The first effect appears to dominate in the ECLIPSE models because SRF strength
9 increases with lifetime. RFaci non-linearities also explain why models simulate weaker SRFs
10 for East Asian than European perturbations. With a more polluted baseline, East Asian aci
11 stands more often at the saturated end of the CCN-cloud albedo relationship, where RFaci is
12 weak (Wilcox et al., 2015). Diversity in RFaci is further increased by variations in the
13 strength of aci (Quaas et al., 2009) and different low cloud climatologies (Jiang et al., 2012).

14 Nitrate aerosol SRFs, whose distributions are shown in Figure S5, have similar optical and
15 cloud nucleus properties as sulphate aerosols yet their SRFs are about 10 times weaker. This
16 weakness is due to two factors. First, formation of ammonium nitrate competes against that of
17 ammonium sulphate, which is favoured by its better thermodynamical stability (Metzger et
18 al., 2002). The efficiency of nitrate precursor reductions therefore depends on regional
19 sulphur dioxide levels. Conversely, the inclusion of nitrate aerosols in OsloCTM2 explains
20 the relatively weak SO₂ SRFs it simulates, because a reduction in SO₂ emissions indirectly
21 favours nitrate formation (Bellouin et al., 2011). In that model, nitrate RFaci offsets 4 to 10%
22 of sulphate RFaci, with larger offsets obtained in Northern Hemisphere winter months.
23 Second, nitrate aerosols are semi-volatile and dissociate back into the gas phase when
24 temperatures increase. Nitrate aerosol formation is therefore hindered during daytime
25 (Dall'Osto et al., 2009), decreasing the ability of nitrate aerosols to interact with radiation.
26 Sulphate aerosols have a more stable diurnal cycle, maximising their radiative forcing
27 efficiency. Although only one ECLIPSE model represents nitrate aerosols, previous studies
28 allow an assessment of likely model diversity in nitrate SRF. AeroCom models with nitrate
29 representations produced estimates of nitrate RF efficiency that range from 60 to 160% of the
30 8-model median of $-155 \text{ W g}[\text{NO}_3]^{-1}$ (Myhre et al., 2013b). Modelled nitrate lifetimes
31 reported for present-day conditions indicate sizeable diversity, with Bellouin et al. (2011)

1 obtaining 3.1 days and Hauglustaine et al. (2014) having 4.6 days (50% longer). Diversity of
2 aerosol-cloud interactions for nitrate is assumed to be similar to the 10% obtained in this
3 study for sulphate aerosols. So a conservative estimate of nitrate SRF diversity is a factor of 2
4 each side of the OsloCTM2 estimate.

5 BC differs from sulphate and OC perturbations in showing no correlation between modelled
6 lifetime and SRF. This lack of correlation has three main causes. First, BC aerosols exert, for
7 a given optical depth and single-scattering albedo, a stronger RFari when located above bright
8 than dark surfaces. Figure S2 shows that the long lifetime of BC in NorESM1 (which may be
9 too long according to Eckhardt et al., 2015) translates into a strong RF over the Arctic for
10 East Asian and Global perturbations. Secondly, BC mass-absorption coefficients (MAC) vary
11 among models because of different assumptions about refractive indices, mixing state, and
12 hygroscopic growth. Globally-averaged BC MAC for ambient conditions is $10.4 \text{ m}^2 \text{ g}^{-1}$ in
13 ECHAM6, $15.7 \text{ m}^2 \text{ g}^{-1}$ in HadGEM3, only $3.8 \text{ m}^2 \text{ g}^{-1}$ in NorESM1, and varies between
14 $7.3 \text{ m}^2 \text{ g}^{-1}$ for hydrophobic and $11.0 \text{ m}^2 \text{ g}^{-1}$ for hydrophilic BC in OsloCTM2. Thirdly,
15 HadGEM3 simulates negative BC SRFs over northern Russia for the Global Summer
16 perturbation (Figure S2) because of complex aerosol mixture effects where perturbations of
17 primary BC emissions also perturb condensation of organic materials. In that model, having
18 fewer primary particles suppresses the gaseous condensation sink and favours the nucleation
19 of new CCNs in pristine regions (Bellouin et al., 2013).

20 The RF due to BC deposition on snow, shown in grey in Figure 2, is only quantified by
21 OsloCTM2. It is a small term globally, and only important for Winter perturbations when
22 snow cover is maximum in the Northern Hemisphere, where fossil-fuel BC sources are mostly
23 located. BC-on-snow RFs represent 15, 20, and 53% of Winter RFari for Global, East Asian,
24 and European perturbations, respectively. The disproportionately strong contribution of the
25 European perturbation is due to its geographical location: in spite of smaller BC emitted mass
26 in Europe, Arctic RF is similar to that of East Asian emission perturbations (Figure S3). So
27 BC-on-snow SRF exerted by the European Winter perturbation is more than 3 times stronger
28 than for the East Asian Winter perturbation and 2 times stronger than for the Global Winter
29 perturbation. Jiao et al. (2014) assessed an offline land surface model with BC deposition
30 rates simulated by AeroCom models, including OsloCTM2, finding that it strongly

1 overestimates BC-in-snow amounts compared to measurements in the Arctic, suggesting a
2 possible overestimation of BC-on-snow SRF in this study.

3 Changes in aerosols may exert rapid adjustments that follow the perturbation to cloud droplet
4 size distributions. Those are not quantified here, because ECLIPSE models do not yet
5 adequately represent the observed dependence of the strength and sign of rapid adjustments
6 on cloud regime (Christensen and Stephens, 2011). In general, confidence in the ability of
7 global models to represent those mechanisms with fidelity is low (Stevens and Feingold,
8 2009). In addition, rapid adjustments are difficult to isolate robustly from internal variability
9 in cloud fraction and top-of-atmosphere radiative fluxes, especially for the small perturbations
10 imposed in this study. However, BC aerosols are unusual among NTCFs because their strong
11 absorption of shortwave radiation is expected to trigger strong rapid adjustments (Koch and
12 Del Genio, 2010), which have been observed in marine stratocumulus regimes (Brioude et al.,
13 2009; Wilcox, 2010). To quantify those adjustments, control and perturbed distributions of
14 BC mass-mixing ratios simulated by OsloCTM2 are prescribed in 30-year, fixed sea-surface
15 temperatures simulations with the Community Earth System Model (CESM) version 1.0.4
16 (Neale et al., 2010). RFari was quantified using multiple calls to the radiation scheme,
17 following Ghan (2013). Because aci are not included in the CAM4 atmospheric component of
18 the CESM, the rapid adjustments from the semi-direct effects of BC are calculated by
19 subtracting its RFari from total ERF. The reference CESM simulation uses BC concentrations
20 taken directly from the reference OsloCTM2 simulation. The changes in BC are therefore
21 scaled before being prescribed in CESM to improve the signal-to-noise ratio between ERF
22 and unforced variability in perturbation simulations. The scaling follows the equation:

$$23 \quad BC_{CESM} = (BC_{REF} - BC_{PERT}) * S + BC_{REF} \quad (Eq. 2)$$

24 where BC_{CESM} are the distributions of BC concentrations prescribed into CESM, BC_{REF} and
25 BC_{PERT} are OsloCTM2's reference and perturbed distributions, respectively. S is the scaling
26 factor and is larger for smaller perturbations (Table 6). So European perturbations are scaled
27 by a factor 500 but RotW perturbations only require a scaling factor of 30. The application of
28 such large scaling factors requires that rapid adjustments from the semi-direct effect scale
29 linearly with the BC perturbation imposed. This has been checked by imposing increasing
30 scaling factors of 15, 50, 150, and 1500 to the East Asian Summer perturbation.
31 Corresponding semi-direct SRFs are -44 ± 121 , -38 ± 40 , -38 ± 12 , and $-35 \pm 1 \text{ mW m}^{-2}$

1 (Tg[BC] yr⁻¹)⁻¹, indicating a satisfactory level of linearity and supporting the application of
2 large scaling factors. Table 6 gives the statistics of the resulting semi-direct SRFs taken over
3 the 30-year CESM simulations. With the exception of the East Asian Winter perturbation,
4 semi-direct SRF is negative, thus opposing the positive BC R_{Fari}. Semi-direct SRFs are
5 weaker in Winter than in Summer perturbations, as expected from a mechanism driven by
6 absorption of shortwave radiation. There are no strong regional variations in semi-direct
7 SRFs. In spite of the large scaling factors imposed, statistics are fragile and 90%-confidence
8 intervals include 0 mW m⁻² for Winter perturbations. It is therefore important to keep in mind
9 that the semi-direct component of BC SRF is even more uncertain than the other components,
10 and may not be significantly different from zero.

11 As discussed in Sect. 2, identification of concentration biases hints at possible systematic
12 errors in SRFs but requires accounting for non-linear dependencies of radiative efficiency
13 with concentrations. ECLIPSE models underestimate sulphate aerosol surface concentrations
14 in Europe because of underestimated SO₂ oxidation rates (Schulz et al., 2015) and in the
15 Arctic because of emissions and transport (Eckhardt et al., 2015). The lack of summer
16 minimum in the Arctic may yield too weak an SRF in that region. For BC, ECLIPSE models
17 generally underestimate BC aerosol surface concentrations in Europe (Schulz et al., 2015) and
18 the Arctic (Eckhardt et al., 2015), possibly because of underestimated emissions. Gadhavi et
19 al. (2015) similarly find that BC emission rates used in ECLIPSE are likely underestimated in
20 India. Absorbing AOD retrievals from AERONET may also indirectly constrain BC
21 concentrations in regions where mineral dust aerosols are not present and where OC aerosols
22 do not strongly contribute to absorption, which may exclude biomass-burning regions (Saleh
23 et al., 2014). However, limitations in the AERONET inversion algorithm (Dubovik et al.,
24 2000) introduce systematic biases towards morning/evening conditions and for thicker
25 plumes. Wang et al. (2015) also showed that the fairly low resolutions of global models like
26 those used in this study induce an artificial negative bias when comparing to AERONET
27 stations in Asia. So the fact that ECLIPSE models underestimate AERONET-retrieved
28 absorbing AOD by more than a factor 2 (Schulz et al., 2015), which could be evidence for
29 underestimated BC concentrations, may be predominantly caused by sampling differences
30 between models and AERONET. In contrast, models overestimate BC radiative efficiency by
31 systematically overestimating BC concentrations at higher altitudes in the remote troposphere

1 (Samset et al., 2014). According to Hodnebrog et al. (2014), the balance between
2 underestimated emissions and overestimated efficiencies translates into BC SRF being too
3 strong by up to a factor 2. For OC, surface concentrations are generally underestimated in
4 Europe (Schulz et al., 2015) and at urban, remote, and marine sites worldwide (Tsigaridis et
5 al., 2014) because of underestimated primary emissions and secondary aerosol formation.
6 Those underestimations may bias OC SRF high, especially for the aci component.

7 **3.2 Methane**

8 As discussed in Sect. 2, methane perturbations have been applied globally and annually,
9 instead of regionally and seasonally. This simplification is motivated by technical
10 considerations, because the long lifetime of methane would necessitate long model spin-ups,
11 and justified by the relatively well mixed nature of methane in the atmosphere compared to
12 shorter-lived species. The regional and seasonal nature of perturbations is therefore quickly
13 lost, all perturbations converging into similar SRFs.

14 The SRF exerted by methane itself is computed analytically on a global average in a four-
15 stage calculation:

16 - First, the methane feedback factor f is derived from each model using Eqs. 2 and 3 of
17 Stevenson et al. (2013), which requires the knowledge of control and perturbed methane
18 burdens, and total methane lifetime τ_{tot} . τ_{tot} accounts for three methane sinks: destruction by
19 OH, which is diagnosed in each model, and losses to the stratosphere and soils, with lifetimes
20 of 120 and 160 years, respectively (Stevenson et al., 2013). ECLIPSE feedback factors range
21 from 1.28 to 1.46 (Table 7), in close agreement with the multi-model mean derived by
22 Holmes et al. (2013).

23 - In a second step, the equivalent methane emission perturbation ΔE is computed as

$$24 \quad \Delta E = \Delta B / (f * \tau_{\text{tot}}) \quad (\text{Eq. 3})$$

25 where ΔB is the change in burden between the control and perturbed simulations.

26 - The third step computes methane RF in each model by inserting control and perturbed
27 methane volume mass-mixing ratios in the formula established by Myhre et al. (1998). The
28 mass-mixing ratio of nitrous oxide (N₂O) used in that calculation is 325 ppb (WMO, 2014).

1 - Finally, methane SRF is computed as the RF divided by ΔE , and increased by 15% to
2 represent the increase in stratospheric water vapour that follows methane oxidation (Myhre et
3 al., 2007b).

4 Methane burdens, lifetimes, and all the global averages involved in computing the methane
5 contribution to total methane SRF in the three ECLIPSE models, are given in Table 7.
6 Simulated methane lifetimes vary by a factor 1.6, reproducing the diversity seen in past
7 studies (Voulgarikis et al., 2013). It is important to note that the diversity in modelled
8 methane SRF is not due to uncertainties in the radiative properties of the molecule, but rather
9 due to the diversity in simulating present-day burdens, which affects the baseline of a non-
10 linear RF.

11 In addition to the SRF exerted by methane itself, components due to perturbations to aerosols
12 and ozone precursors contribute to total methane SRF (Figure 3). Aerosol and ozone RFs are
13 derived using the methods described in Sect. 2. The aerosol component arises from the
14 increase in OH that follows the decrease in CH₄ concentrations, promoting SO₂ oxidation into
15 sulphate aerosols that contribute a negative RF. That contribution is very diverse among
16 models, varying from weakly negative in OsloCTM2 to strongly positive in HadGEM3. The
17 OsloCTM2 value is from a simplified calculation, which only represents ari by using
18 distributions of radiative forcing efficiencies instead of the full radiative transfer calculations
19 normally used. Three other aspects of the models increase the diversity in estimates of aerosol
20 contributions to methane SRF. Firstly, the size of the relative increase in global OH burden
21 that follows the decrease in methane concentrations is larger in HadGEM3, at +7%, than in
22 NorESM1 and OsloCTM2, at +4.5% and +4.6%, respectively. Secondly, other limitations
23 restrict the aerosol response in some models, but not others. For example, NorESM simulates
24 aerosol SRFs of differing signs (Figure S6), which indicate different responses of local
25 chemistry, possibly mediated by changes in oxidation pathways by O₃ and H₂O₂. In
26 HadGEM3 however, aerosol SRF is uniformly positive across the globe (Figure S6),
27 indicating that once OH is increased, no further limitation restricts the size of the aerosol
28 response. The realism of those responses are difficult to confirm from observations, as
29 evidence for changes in the oxidising capacity of the atmosphere are lacking. Thirdly, the
30 inclusion of nitrate aerosols in OsloCTM2 counteracts the sulphate aerosol response, because

1 increases in ammonium sulphate aerosol formation are detrimental to ammonium nitrate
2 aerosol formation.

3 In contrast to the diversity seen in the aerosol component of total methane SRF, all three
4 models simulate ozone contributions to methane SRF close to one third of the SRF of
5 methane itself. This chemical feedback is therefore in good agreement among models, and is
6 proportional to the size of the methane perturbation. Figure S7 shows that the models also
7 agree well on the geographical distribution of the ozone SRF, with a maximum at the tropical
8 boundaries.

9

10 **3.3 Ozone precursors**

11 Figure 4 shows globally- and annually-averaged SRF for nitrogen oxide, volatile organic
12 compounds, and carbon monoxide perturbations in the three ECLIPSE models with
13 tropospheric ozone chemistry schemes. The methane and primary-mode ozone SRF are
14 calculated as global averages only, by multiplying the change in methane burden due to its
15 reaction with OH by a methane radiative forcing efficiency (RFE) of $0.363 \text{ mW m}^{-2} \text{ ppbv}^{-1}$
16 (Table 8.A.1 of Myhre et al., 2013a). Primary-mode ozone RFE is computed as the ratio of
17 ozone RF to total methane burden change in the methane perturbation simulations (see
18 Sect. 3.2). That RFE is more easily expressed as a fraction of methane RFE, with good
19 agreement among ECLIPSE models: 0.396 for HadGEM3, 0.385 for NorESM1, and 0.395 for
20 OsloCTM2.

21 For all models, regions and seasons, total NO_x SRF is negative and CO SRF is positive.
22 Models disagree on the sign of VOC SRF. SRF components are region- and season-
23 dependent, but the dependence of net SRF is less pronounced because the short-lived ozone
24 and aerosol contributions compensate each other. Dependencies of CO SRFs on region and
25 season are worth noting: an increased methane contribution makes Winter perturbations more
26 efficient at exerting a CO SRF than Summer perturbations, and models also agree that East
27 Asian perturbations exert slightly stronger SRFs than European perturbations because of a
28 stronger SRF by ozone. East Asian ozone exerts a stronger RF per unit ozone burden because
29 of higher NO_x background in that region but also because it is closer to the Equator, where
30 more sunlight leads to a more active photochemistry (Berntsen et al., 2006).

1 In terms of RF contributions, models are in generally good agreement for the ozone
2 contribution both on a global average (Figure 4) and patterns (Figures S9, S11, and S13), with
3 ozone RF being mostly located in the latitude band of the perturbed region. The VOC
4 perturbations are an exception and exhibit model diversity in global averages, echoing the
5 complexity and diversity of VOC chemistry. Decreasing VOC emissions leads to a decrease
6 in their oxidation products, CO and O₃, therefore increasing OH and decreasing CH₄
7 concentrations (Lin et al., 1988). Different VOCs have different photochemical O₃ creation
8 potentials (Derwent et al., 2001; Young et al., 2013). The three ECLIPSE models include a
9 different number of VOC species. The model with the largest number of VOC species is
10 OsloCTM2, with 40 species: 28 in the tropospheric chemistry scheme and 12 in the secondary
11 organic aerosol scheme. Its broader range of VOC lifetimes and ozone production potentials
12 means that it simulates the strongest ozone SRF. HadGEM3 is at the other end of the range of
13 species considered and simulates the weakest ozone SRF. For CO, all models agree that the
14 methane SRF contribution is larger than that of short-lived ozone changes. The opposite is
15 true for VOC, where the ozone contribution dominates. This difference stems from the
16 weaker ozone production potential of CO, caused by slower reaction rates (e.g. Bowman,
17 1995).

18 There is a good agreement on methane and primary-mode ozone contributions between
19 OsloCTM2 and NorESM1 but HadGEM3 simulates a weaker SRF. This is consistent with
20 results from the methane perturbation (Sect. 3.2 and Table 7) and similarly caused by
21 different baseline methane levels.

22 Models strongly disagree on the sign and magnitude of the aerosol contribution. For NO_x,
23 that contribution is generally negative, but NorESM1 also simulates positive contributions,
24 especially in Winter perturbations. OsloCTM2 and HadGEM3 disagree on the season and
25 region where the strongest aerosol contributions are exerted. Figure S8 shows that those
26 disagreements stem from differences in regional responses. Both HadGEM3 and NorESM1
27 show positive aerosol RFs centred on the regions being perturbed, caused by a decrease in
28 sulphate aerosol formation through OH oxidation because OH levels are decreased. The SO₂
29 not oxidised and not deposited is transported downwind of the perturbed region, where it
30 promotes sulphate aerosol formation in the absence of oxidant limitation: in those regions,
31 both models simulate negative aerosol RFs. The balance between regions of positive and

1 negative aerosol RF varies depending on the model, the perturbed region, and the season. In
2 contrast, OsloCTM2 does not simulate this dipole of responses: its aerosol contribution is
3 negative almost everywhere on the globe. The representation of nitrate aerosols explains that
4 difference of behaviour compared to the other models. Nitrate exerts between 50 and 95% of
5 R_{Fari} to NO_x perturbations in OsloCTM2, with largest contributions in Northern Hemisphere
6 winter months, adding a negative RF in, and downwind of, the perturbed regions. This brings
7 the total aerosol SRF for NO_x perturbations firmly into negative values.

8 For VOC perturbations, the aerosol contribution is negative in NorESM1 and OsloCTM2 but
9 generally positive in HadGEM3. VOC perturbations perturb aerosols via secondary organic
10 aerosol formation. The strength of this link varies strongly between models because of the
11 heterogeneity in the number and type of VOCs represented. Although HadGEM3 agrees with
12 NorESM1 and OsloCTM2 that aerosol RF is negative above the perturbed regions (Figure
13 S10), those negative RFs are weak and therefore easily compensated on a global average by
14 noisy positive contributions in regions where the aerosol internal mixture has been perturbed
15 (e.g. north-western Russia, Indonesia, South America). Observational constraints on such
16 internal mixture perturbations are lacking, so it is not currently possible to assess the realism
17 of HadGEM3's response. The weakness of aerosol SRF in OsloCTM2 compared to NorESM1
18 is due to the representation of nitrate aerosols, which counteract part of the RF exerted by
19 changes in sulphate aerosols, but also to a weaker R_{Faci} contribution.

20 For CO perturbations, both NorESM1 and OsloCTM2 simulate relatively weak contributions
21 of aerosols to CO SRF. The contribution simulated by OsloCTM2 is negative because the
22 positive RFs exerted by sulphate and secondary organic aerosols are more than compensated
23 by a negative RF by nitrate aerosols. HadGEM3 simulates a relatively strong response of
24 aerosols to CO perturbations (Figure S12), but that is because biomass-burning emissions
25 were also perturbed in this model. NorESM1 and OsloCTM2 only perturbed fossil-fuel
26 combustion emissions, and the results suggest that links between CO and aerosols are stronger
27 for biomass-burning sources. However, other sources of diversity, including the
28 representation of atmospheric chemistry, could also explain the differences in behaviour
29 between HadGEM3 and the other participating models.

30

1 **3.4 Shipping sector**

2 Figure 5 shows globally- and annually-averaged SRF for all species (SO₂, BC, OC, CH₄,
3 NO_x, VOC, and CO) emitted by the shipping sector. ECHAM6 lacks a tropospheric ozone
4 chemistry scheme, and therefore only simulates the aerosol contribution, and furthermore
5 diagnoses R_{Fari} only. OsloCTM2 is the only model that includes BC-on-snow RF and
6 quantifies BC semi-direct RF (Sect. 3.1). Models agree qualitatively that ozone contributes a
7 positive SRF and methane, primary-mode ozone, and aerosols provide a negative SRF.
8 Methane and primary-mode ozone SRFs, which are computed as described in Sect. 3.2, are
9 mainly driven by emissions of NO_x. The SRF contributed by short-lived changes in ozone are
10 in good agreement among models, both in terms of global averages (Figure 5) and
11 geographical patterns (Figure S16), with maxima in the Tropics. ECLIPSE models may
12 overestimate that contribution, however, because assuming instantaneous dilution of
13 emissions over their grid boxes, instead of representing ship plumes, is known to lead to an
14 overestimate of ozone production by NO_x (Paoli et al., 2011). BC-on-snow (see also
15 Figure S15) and BC semi-direct SRF, which are quantified from OsloCTM2 simulations as
16 described in Sect. 3.2, are weak. Methane SRF is a large contribution to shipping SRF
17 because ships emit in pristine environments, where ozone precursor emissions have a
18 relatively larger impact than in polluted regions.

19 Models agree that aerosols dominate shipping SRF, but disagree on the strength of that
20 contribution, for the same causes listed above, and notably different lifetimes, different
21 strengths of R_{Faci}, and different treatment of the aerosol mixing state. Geographical patterns
22 are similar among models and reflect main shipping routes (Figure S14). NorESM1 shows a
23 region of positive aerosol RF in the Arctic, caused by the long-range transport of its long-
24 lived BC, which may not be realistic because that model overestimates BC Arctic
25 concentrations in the Summer (Eckhardt et al., 2015).

26 27 **4 Matrix of specific radiative forcing**

28 This section describes how the individual model results described in Sect. 3 can be
29 summarised into the more useful best estimate and range. All global numbers by individual
30 models are given in Supplementary Materials, to allow users to make other choices.

1 For each regional and seasonal perturbation by a NTCF, best estimates of SRF are provided
2 for each RF mechanism: aerosols (sum of RFari and RFaci), BC deposition on snow, BC
3 rapid adjustments to semi-direct effects, short-lived changes in tropospheric ozone
4 concentrations, methane, and primary-mode ozone. The best estimate on net SRF is the sum
5 of the best estimates of all RF mechanisms that are relevant to the NTCF considered. Inter-
6 model diversity is represented by an interval ranging from the weaker SRF, obtained by
7 adding the weaker estimates of all RF mechanisms, to the stronger SRF, obtained by adding
8 the stronger estimates of all RF mechanisms. Best estimates of RF of BC deposition on snow
9 and BC rapid adjustments from semi-direct effects are available from only one model, so are
10 also taken to represent high and low estimates. It is however important to note that the
11 statistics on BC adjustments from semi-direct effects are not robust and that it may in fact not
12 be significantly different from zero for the Winter perturbations, as discussed in Sect. 3.1.

13 It can be argued that the models that fail to provide realistic simulations of key aspects of
14 NTCF distributions and RF mechanisms should be discarded. For example, Shindell et al.
15 (2013) screen the 10 models that participated in ACCMIP for their ability to reproduce
16 observed total AOD and its recent trend, leading to a reduction in inter-model diversity. Such
17 a screening is not applied here because models do not exhibit uniform skill at reproducing
18 aerosol or ozone distributions: a model that could be considered best in one region often
19 shows poorer skill in another. Nevertheless, decisions are required here on the inclusion of
20 models that do not diagnose RFaci, or simulate long BC lifetimes, or lack nitrate aerosols, or
21 simulate complex aerosol-chemistry responses. The decisions are:

22 - For RFaci, ECHAM6 is not included in best estimates of aerosol SRF because it does not
23 diagnose aci, which according to the other models is the often dominant contribution to total
24 aerosol RF. It is possible that RFaci is in fact compensated by rapid adjustments in cloud
25 liquid water path (e.g. Christensen and Stevens, 2011), meaning that ECLIPSE models
26 overestimate the strength of aerosol SRF. However, there is currently no evidence that such
27 compensation happens on a global scale.

28 - For BC lifetimes, a possible decision would be to discount models with BC lifetimes longer
29 than about 4 days, which is the lifetime obtained by constraining BC mass concentration
30 profiles with aircraft observations (Wang et al., 2014b; Hodnebrog et al., 2014). That decision
31 would give more weight to the aerosol SRF simulated by ECHAM6 and HadGEM3.

1 However, comparisons to surface observations in the Arctic suggest that ECHAM6 and
2 HadGEM3 underestimate BC concentrations in that region (Eckhardt et al., 2015), perhaps
3 because aerosols do not stay long enough in the atmosphere to be transported to the Arctic in
4 those two models. Reconciling mixed conclusions from different indirect observational
5 constraints on lifetime is therefore warranted. In the meantime, no model is discounted in this
6 study when producing the best ECLIPSE model estimate and range of BC SRF. Still, the
7 tendency of models to put BC too high in the atmosphere needs to be kept in mind, as it leads
8 to an overestimated SRF.

9 - For nitrate, the descriptions of results for the SO₂ (Sect. 3.1) and ozone precursor (Sect. 3.3)
10 perturbations note the importance of co-variations in nitrate aerosols. Those are only
11 represented in OsloCTM2 but are crucial in that model in determining the strength, and on
12 occasions even the sign, of aerosol SRF. For that reason, it is decided here to add the nitrate
13 SRF simulated by OsloCTM2 to the aerosol SRF of the other models. This solution is crude,
14 as it is known that model diversity in simulating nitrate distributions is large (Myhre et al.,
15 2013b) and a correlation between sulphate and nitrate RF can be expected from their links
16 through ammonium. But in the absence of a solid understanding of those correlations, the
17 solution adopted here has the merit of simplicity and prevents misleading overcorrections.

18 - For aerosol-chemistry interactions, HadGEM3 simulates complex responses of aerosols to
19 ozone precursor perturbations. This is particularly true of VOC perturbations (Sect. 3.3),
20 where HadGEM3 simulates a positive SRF when NorESM1 and OsloCTM2 agree on a
21 negative contribution. At this stage, the realism of HadGEM3's response cannot be confirmed
22 by observations, but nor can it be challenged. It is therefore decided to include HadGEM3 in
23 the best estimate and range of VOC SRF, with the caveat that its behaviour is peculiar.

24 Figure 6 shows the resulting best SRF estimate for all perturbations. Best estimates for each
25 mechanism are shown in colour. Best estimates for the net SRF are shown as black bars, with
26 the range from weaker to stronger estimates represented as whiskers. The range for NH₃
27 perturbations, which have been quantified from one model only, is assumed to be a factor 2
28 (Sect. 3.1). Model diversity ranges are often sizeable, but rarely include zero, indicating that
29 models generally agree on the sign of the SRF of a given NTCF. The sign of the SRF exerted
30 by VOC perturbations is however unclear because it depends on the strength and sign of

1 aerosol responses, including secondary organic aerosols. The best estimate of VOC SRF is
2 positive, but individual models cannot agree on the sign and the diversity range is large.

3 Quantitatively, best estimates of BC SRF are the strongest of all NTCFs, even after
4 accounting for rapid adjustments from semi-direct effects. Aerosol SRFs are generally
5 stronger than ozone precursor SRFs, with the exception of NH₃ perturbations, which exert
6 weak SRF because of competition with ammonium sulphate aerosol formation and because
7 the diurnal cycle of nitrate aerosol formation is unfavourable to ari (Sect. 3.1). NO_x exerts the
8 strongest SRF of all ozone precursor perturbations, although VOC perturbations are
9 potentially as strong but much more uncertain. Shipping SRF is strong because of strong
10 contributions by aerosols and methane.

11 The best estimates of this study are included in Table 1 for convenient comparison to previous
12 studies. This study suggests a revision towards stronger SRFs for SO₂ and OC perturbations
13 because of the inclusion of R_Faci. In contrast, this study's BC SRF is not very different from
14 that derived by studies that consider ari only, because the inclusion of aci, deposition on
15 snow, and rapid adjustments from semi-direct effects contributes only a weakly positive, and
16 even at times negative, SRF. The BC SRF estimated in this study sits in the middle of the
17 range proposed by Bond et al. (2013), in spite of their increase in emissions to correct for
18 perceived underestimations in absorbing aerosol optical depth. This is because BC radiative
19 efficiency for ari is fairly linear with emissions so SRF estimates are not strongly affected by
20 BC emission changes. For methane and ozone precursor perturbation, the study agrees well
21 with previous efforts in estimating the methane contribution. The SRF exerted by short-lived
22 perturbations to ozone concentrations is generally revised upward. Compared to Fry et al.
23 (2012), this study quantifies aerosol responses to ozone precursor perturbations for more
24 aerosol species and RF mechanisms, especially including aci. Those additional components
25 put the aerosol contribution more firmly into negative values for NO_x and VOC
26 perturbations, but with increased model diversity. For CO perturbations, Fry et al. (2012),
27 which only accounted for sulphate R_Fari, found that aerosols contributed a negative SRF.
28 This study finds that that contribution may in fact be positive because nitrate aerosols more
29 than compensate for the sulphate RF.

30

1 **4.1 Seasonality**

2 For all perturbations, SRF best estimates are given for emission reductions applied in two
3 periods, May-Oct and Nov-Apr, which are labelled in Figure 6 Summer and Winter,
4 respectively, because emission perturbations are predominantly located in the Northern
5 Hemisphere. The seasonality of methane perturbations was not considered because the time of
6 emission becomes quickly irrelevant compared to the long residence time of methane in the
7 atmosphere.

8 Aerosol primary and precursor perturbations are largely located in the Northern Hemisphere
9 and Summer emission reductions exert strong SRFs because the RF mechanisms act mostly
10 on shortwave radiation. For RFari, anthropogenic aerosols are predominantly located in the
11 accumulation mode, at sizes which interact most efficiently with shortwave radiation. For
12 RFaci, changes to cloud albedo operate in the shortwave spectrum only, although BC semi-
13 direct SRF has a longwave component. In addition to RF mechanisms, chemical production
14 and sinks (mainly from precipitation) also influence seasonality. SO₂ photolysis is an example
15 of a reaction favoured by higher, summertime, shortwave radiative fluxes. Temperature is
16 also a factor, especially in nitrate aerosol formation, which is favoured by colder
17 temperatures. This dependence explains the unusual seasonality of NH₃ perturbations, which
18 exert stronger SRFs in Winter perturbations for East Asia and on a global average. The fact
19 that European perturbations behave differently is linked to the lower sulphate aerosol levels in
20 Europe, reducing their ability to limit nitrate formation in both summer and winter months.

21 The SRF of ozone precursor perturbations is exerted across both the shortwave and longwave
22 spectra, so its seasonality is not as strong as for aerosol perturbations and the details of ozone
23 formation pathways are important. Figure 6 shows that Winter NO_x perturbations exert
24 stronger SRFs, except for European perturbations. The seasonality of NO_x RF depends on the
25 level of cancellation between the positive ozone contribution and the negative methane
26 contribution. Derwent et al. (2008) found using a CTM that there are no simple relationships
27 that explain that competition, which also varies regionally. Our results replicate that
28 complexity. CO Winter perturbations are consistently stronger than Summer perturbations,
29 but differences are generally small. Finally, VOC perturbations may have a seasonality where
30 Summer perturbations are stronger than Winter perturbations, but model diversity is large so
31 the seasonality is uncertain.

1

2 **4.2 Latitudinal variations**

3 Figures 7a and 7b show best estimates and ranges of SRF for aerosols and ozone precursors,
4 respectively, across four latitude bands: 90N—60N, 60N—28N, 28N—28S, and 28S—90S.
5 Those bands have been chosen to represent the Arctic, mid-latitudes, Tropics, and Southern
6 Hemisphere extratropical latitudes, respectively. The Southern Hemisphere is less resolved
7 than the Northern Hemisphere because anthropogenic emissions are predominantly located in
8 the latter. European emission perturbations are entirely located in the second band (60N—
9 28N). East Asian emission perturbations also include the northern portion of the third band
10 (28N—28S). RotW and shipping perturbations are located across all four bands, but again
11 with Northern Hemisphere emissions having more weight.

12 Latitudinal averaging of RF is done on the annual distributions shown as Supplementary
13 Figures. SRF is then computed by normalising by the globally-averaged emission change: so
14 for a given perturbation, both global and latitudinal SRFs share the same normalisation
15 factors. Annual distributions are however not available for methane RF and BC rapid
16 adjustments to semi-direct effects. Methane RF has been computed as a global average only
17 (see Sect. 3.2) because it is assumed here to be uniformly distributed across the globe, which
18 is justified on an annual basis by the well-mixed nature of methane. BC rapid adjustments are
19 associated with noisy distributions (see Sect. 3.1), so there is low confidence in the
20 significance of regional patterns. They are assumed here to follow the same latitudinal
21 distribution of BC R_{Fari}, which is justified by the close physical links between the two RF
22 processes.

23 Figures 7 show that although SRF is typically stronger in the latitude band where the emission
24 perturbation is applied, it is not confined to that latitude band. This behaviour is expected
25 from atmospheric transport, and has been found previously in other modelling studies (e.g.
26 Shindell and Faluvegi, 2009). European aerosol and precursor perturbations affect the Arctic
27 in a sizeable way. The BC European and Global Winter perturbations may even exert a
28 stronger positive SRF in the Arctic than in mid-latitudes where the perturbations are located,
29 because of the added positive contribution of BC-on-snow RF. The SRF exerted by East
30 Asian perturbations is more confined to mid-latitudes, because atmospheric transport

1 preferentially advects the perturbations towards the Pacific Ocean rather than the Arctic,
2 especially in Winter perturbations (Figure S2).

3 Ozone precursor perturbations (Figure 7b) tend to be more diffuse than their aerosol
4 counterparts, in part because of the longer lifetime of ozone in ECLIPSE models (Table 5) but
5 also because perturbations to OH lifetime are more efficient in the Tropics (Berntsen et al.,
6 2006). SRF of ozone precursor perturbations are therefore strong in Northern Hemisphere
7 mid-latitudes, where the perturbations are located, and the Tropics. For European and East
8 Asian perturbations, the Arctic is generally associated with weaker SRFs, except for CO,
9 which is associated with more spatially uniform SRFs because methane RF is the main
10 contributor. The SRF of shipping sector perturbations peaks in the Northern Hemisphere,
11 where the busiest shipping lanes are located.

12

13 **5 Conclusion**

14 This study provides NTCF SRFs by using ECLIPSE model simulations by four general
15 circulation and chemistry-transport models: ECHAM6, HadGEM3, NorESM1, and
16 OsloCTM2. SRFs are given for eight NTCFs, four regions or sectors, and six RF mechanisms.
17 The four regions are Europe, East Asia, global average, and the shipping sector. The eight
18 NTCFs or NTCF precursors are SO₂, BC, OC, NH₃, methane, NO_x, CO, and VOC. NH₃
19 perturbations were applied in OsloCTM2 only, which includes a representation of nitrate
20 aerosols. The six RF mechanisms are aerosols (both ari and aci), BC deposition on snow, BC
21 rapid adjustments from semi-direct effects, short-lived ozone changes, methane, and primary-
22 mode ozone. OsloCTM2 is the only model used to estimate BC deposition on snow and BC
23 rapid adjustments from semi-direct effects. ECHAM6 does not simulate ozone chemistry, so
24 does not provide SRFs for the last three RF mechanisms on the list.

25 Models generally agree on the sign of the total SRF of a given NTCF, except for VOC
26 although its best estimate is positive. Quantitatively, models are more diverse. That diversity
27 has multiple and complex roots, but four important aspects stand out.

- 28 - Diversity in modelled NTCF lifetimes is large, with longest lifetimes being 1.5 to 2.5
29 times longer than the shortest lifetimes depending on NTCF. Differences in lifetime
30 affect both the reach of long-range transport and the reference baseline.

- 1 - The unperturbed baseline causes diversity for non-linear RF mechanisms, such as
2 RFaci and methane RF. It is also a common cause for regional differences in SRF.
- 3 - The number of species represented varies among models. Nitrate and secondary
4 aerosols modulate the strength of the SRF exerted by SO₂, NO_x, VOC, and CO
5 perturbations, but are not included in all models, causing potentially misleading results
6 in models where those aerosol species are absent. Models that include VOC emissions
7 also account for a different number and type of VOC species.
- 8 - Interactions between aerosols and chemistry, and particularly aerosol responses to
9 changes in the oxidising capacity of the atmosphere and secondary organic aerosol
10 formation, affect the strength, possibly even the sign, and the seasonality of SRF. The
11 strength of those interactions differs among models.

12 Harmonising modelling capabilities, and deriving observational constraints on modelled
13 lifetimes (e.g. Kristiansen et al., 2016) and responses of OH concentrations to chemistry
14 perturbations will be useful in reducing model diversity while also quantifying model skill at
15 simulating atmospheric composition with fidelity. Other causes of diversity include different
16 aerosol optical properties, including BC absorbing properties (e.g. Myhre et al., 2013b);
17 different vertical profiles (e.g. Samset et al., 2013); different cloud processes, which affect the
18 strength of RFaci (e.g. Quaas et al., 2009); and host model considerations, such as the use of
19 different radiative transfer schemes (Stier et al., 2013) and different simulations of horizontal
20 and vertical cloud distributions.

21 From a climate mitigation point of view, the key messages from the present study are that:

- 22 - Including aerosol-cloud interactions increases the magnitude of the SRF for SO₂ and
23 OC perturbations compared to previous studies. The NTCFs exerting the strongest
24 SRFs are well identified, with robust rankings across models. SRF exerted by aerosol
25 perturbations is up to an order of magnitude stronger than methane and ozone
26 precursor perturbations, although the latter are associated with larger emission rates.
- 27 - Perturbing VOC emissions is an unreliable mitigation option because different models
28 disagree on the sign of the resulting SRF.
- 29 - It is more efficient to perturb European or shipping aerosol emissions than East Asian
30 emissions because East Asia has a more polluted baseline which saturates RFaci and
31 dampens the impact of emission reductions. So improving air quality without

1 weakening the negative RF of aerosols is easier in the more polluted regions. The
2 regional dependence of ozone precursor SRF is more complex, and no systematic rule
3 is found, in common to previous studies (Derwent et al., 2008). The regional
4 dependencies of CO perturbations are however weaker than those of NO_x and VOC,
5 as also found by Fry et al. (2012).

- 6 - SRFs generally peak in the latitude band where the perturbation is applied, although
7 other regions, notably the Arctic, are affected through long-range transport. In that
8 respect, reducing European BC Winter emissions seems an efficient way to minimise
9 positive RF in the Arctic because of the added contribution of BC deposition on snow.
- 10 - The SRF of Summer perturbations is stronger than that of Winter perturbations for
11 most NTCFs, with the notable exception of ammonia perturbations. The SRF
12 seasonality of aerosol perturbations is more pronounced than that of ozone precursor
13 perturbations, and less complex and regionally dependent. Minimising positive
14 anthropogenic RF by NTCF mitigation is thus best done by reducing summertime
15 emissions of species with positive SRFs, like BC, and wintertime emissions of species
16 with negative SRFs, like SO₂.

17 Aamaas et al. (2015) provide an example of how the ECLIPSE matrix of SRF can be used to
18 derive climate metrics able to estimate the climate impact of mitigation policies. Baker et al.
19 (2015) discuss the climate impacts simulated by climate models forced by future emission
20 scenarios based on the ECLIPSE SRF matrix, concluding that the climate response to
21 reductions of BC and OC emissions is not clearly discernible.

22 The SRF matrix presented does not include rapid adjustments to all RF mechanisms so is not
23 a matrix of specific ERF, which would arguably have been more useful. Unfortunately,
24 quantifying ERF is more challenging than the already challenging task of quantifying RF,
25 especially for the small regional and seasonal perturbations considered here. The challenge is
26 to distinguish, in a statistically robust way, rapid adjustments from internal variability. The
27 only rapid adjustment considered in this study is from the semi-direct effect of BC aerosols,
28 and the statistics are fragile. Nudging of temperature and wind speeds have shown promise in
29 decreasing the size of internal variability (Kooperman et al., 2012), but whether that method
30 also suppresses rapid adjustments is unknown. One possible variation of that method is to
31 allow temperature to adjust freely to semi-direct effects, while wind speeds remain nudged to

1 decrease internal variability between perturbed and unperturbed simulations. Implemented in
2 HadGEM3, that method successfully reproduces the globally-averaged seasonality of ERF
3 and subsequent precipitation changes simulated by free-running simulations (Figures S17 and
4 S18). The simulations required to do so are 6 times shorter and have better statistics. This
5 encouraging result holds for a variety of RF mechanisms, including a doubling of carbon
6 dioxide concentrations and RF ari and aci. However, that method assumes that
7 thermodynamical and dynamical responses are separated, at least over rapid adjustment
8 timescales, which remains to be demonstrated.

9

10 **Data availability**

11 Supplementary Materials include spreadsheets giving all globally-averaged numbers for all
12 perturbation simulations and all radiative forcing mechanisms, by all models.

13

14 **Acknowledgements**

15 The research and simulations described in this study were funded by the European Union
16 Seventh Framework Programme (FP7/2007-2013) under grant agreement number 282688 –
17 ECLIPSE. The research team based at the University of Reading acknowledges use of the
18 MONSooN supercomputing system, a collaborative facility supplied under the Joint Weather
19 and Climate Research Programme, which is a strategic partnership between the UK Met
20 Office and the UK Natural Environment Research Council. The University of Leipzig team
21 acknowledges additional funding by the European Research Council (QUAERERE,
22 GA 306284) and computing time from the German Climate Computing Centre (DKRZ). The
23 CICERO team acknowledges additional funding from the Research Council of Norway
24 through the NetBC (number 244141) and SLAC (number 208277) projects.

25

26 **Author contribution**

27 N. Bellouin, G. Myhre, and J. Quaas designed the experiments as part of the ECLIPSE
28 project. N. Bellouin, L. Baker, Ø. Hodnebrog, D. Olivié, R. Cherian, C. Macintosh, B.
29 Samset, and A. Esteve ran the experiments or radiative transfer calculations, and analysed the

1 data sets. B. Aamaas provided additional data analysis in the perspective of climate metrics
2 users. N. Bellouin prepared the manuscript with contributions from all co-authors.

3

4 **References**

5 Aamaas, B., Berntsen, T. K., Fuglestvedt, J. S., Shine, K. P., and Bellouin, N.: Multimodel
6 emission metrics for regional emissions of short lived climate forcers, *Atmos. Chem. Phys.*
7 *Discuss.*, 15, 26089-26130, doi:10.5194/acpd-15-26089-2015, 2015.

8 Baker, L. H., Collins, W. J., Olivie, D. J. L., Cherian, R., Hodnebrog, Ø., Myhre, G., and
9 Quaas, J.: Climate responses to anthropogenic emissions of short-lived climate pollutants,
10 *Atmos. Chem. Phys.*, 15, 8201-8216, doi:10.5194/acp-15-8201-2015, 2015a.

11 Bellouin, N., Rae, J., Jones, A., Johnson, C., Haywood, J., and Boucher, O.: Aerosol forcing
12 in the Climate Model Intercomparison Project (CMIP5) simulations by HadGEM2-ES and the
13 role of ammonium nitrate. *J. Geophys. Res.*, 116, D20206, doi:10.1029/2011JD016074, 2011.

14 Berntsen, T., Fuglestvedt, J., Myhre, G., Stordal, F., and Berglen T.F.: Abatement of
15 Greenhouse Gases: Does Location Matter? *Climatic Change*, 74, 4, 377—411,
16 doi:10.1007/s10584-006-0433-4, 2006.

17 Bentsen, M., Bethke, I., Debernard, J. B., Iversen, T., Kirkevåg, A., Seland, Ø., Drange, H.,
18 Roelandt, C., Seierstad, I. A., Hoose, C., and Kristjánsson, J. E.: The Norwegian Earth
19 System Model, NorESM1-M – Part 1: Description and basic evaluation of the physical
20 climate, *Geosci. Model Dev.*, 6, 687–720, doi:10.5194/gmd-6-687-2013, 2013.

21 Bond, T.C., S.J. Doherty, D.W. Fahey, P.M. Forster, T. Berntsen, B.J. DeAngelo, M.G.
22 Flanner, S. Ghan, B. Kärcher, D. Koch, S. Kinne, Y. Kondo, P.K. Quinn, M.C. Sarofim, M.G.
23 Schultz, M. Schulz, C. Venkataraman, H. Zhang, S. Zhang, N. Bellouin, S.K. Guttikunda,
24 P.K. Hopke, M.Z. Jacobson, J.W. Kaiser, Z. Klimont, U. Lohmann, J.P. Schwarz, D. Shindell,
25 T. Storelvmo, S.G. Warren, and C.S. Zender. Bounding the role of black carbon in the climate
26 system: A scientific assessment. *J. Geophys. Res.*, 118, 5380-5552, doi:10.1002/jgrd.50171,
27 2013.

28 Boucher, O., D. Randall, P. Artaxo, C. Bretherton, G. Feingold, P. Forster, V.-M. Kerminen,
29 Y. Kondo, H. Liao, U. Lohmann, P. Rasch, S.K. Satheesh, S. Sherwood, B. Stevens and X.Y.

1 Zhang, 2013: Clouds and Aerosols. In: Climate Change 2013: The Physical Science Basis.
2 Contribution of Working Group I to the Fifth Assessment Report of the Intergovernmental
3 Panel on Climate Change [Stocker, T.F., D. Qin, G.-K. Plattner, M. Tignor, S.K. Allen, J.
4 Boschung, A. Nauels, Y. Xia, V. Bex and P.M. Midgley (eds.)]. Cambridge University Press,
5 Cambridge, United Kingdom and New York, NY, USA, 2013.

6 Bowman, F.M.: A multi-parent assignment method for analyzing atmospheric chemistry
7 mechanisms. *Atmos. Environ.*, 39, 14, 2519—2533, doi:10.1016/j.atmosenv.2004.12.040,
8 2005.

9 Brioude, J., Cooper, O. R., Feingold, G., Trainer, M., Freitas, S. R., Kowal, D., Ayers, J.K.,
10 Prins, E., Minnis, P., McKeen, S. A., Frost, G. J., and Hsie, E.-Y.: Effect of biomass burning
11 on marine stratocumulus clouds off the California coast, *Atmos. Chem. Phys.*, 9, 8841-8856,
12 doi:10.5194/acp-9-8841-2009, 2009.

13 Carslaw, K.S., L.A. Lee, C.L. Reddington, K.J. Pringle, A. Rap, P.M. Forster, G.W. Mann,
14 D.V. Spracklen, M.T. Woodhouse, L.A. Regayre, and J.R. Pierce, Large contribution of
15 natural aerosols to uncertainty in indirect forcing, *Nature*, 503, 67–71,
16 doi:10.1038/nature12674, 2013.

17 Christensen, M.W., and Stephens, G.L.: Microphysical and macrophysical responses of
18 marine stratocumulus polluted by underlying ships: Evidence of cloud deepening, *J. Geophys.*
19 *Res.*, 116, D03201, doi:10.1029/2010JD014638, 2011.

20 Collins, W.D.: Parameterization of generalized cloud overlap for radiative calculations in
21 general circulation models, *J. Atmos. Sci.*, 58, 3224–3242, doi:10.1175/1520-0469(2001)058,
22 2001.

23 Dall'Osto, M., Harrison, R. M., Coe, H., Williams, P. I., and Allan, J. D.: Real time chemical
24 characterization of local and regional nitrate aerosols, *Atmos. Chem. Phys.*, 9, 3709-3720,
25 doi:10.5194/acp-9-3709-2009, 2009.

26 Dalsøren, S. B., Ø. Endresen, I. S. A. Isaksen, G. Gravir, and E. Sørgård: Environmental
27 impacts of the expected increase in sea transportation, with a particular focus on oil and gas
28 scenarios for Norway and northwest Russia, *J. Geophys. Res.*, 112, D02310,
29 doi:10.1029/2005JD006927, 2007.

1 Derwent, R. G., Jenkin, M. E., Saunders, S. M., and Pilling, M. J.: Characterization of the
2 reactivities of volatile organic compounds using a master chemical mechanism, *J. Air Waste*
3 *Ma.*, 51, 5, 699-707, doi:10.1080/10473289.2001.10464297, 2001.

4 Derwent, R.G., D.S. Stevenson, R.M. Doherty, W.J. Collins, M.G. Sanderson, and C.E.
5 Johnson: Radiative forcing from surface NO_x emissions: spatial and seasonal variations,
6 *Climatic Change*, 88, 385—401, doi:10.1007/s10584-007-9383-8, 2008.

7 Dubovik, O., A. Smirnov, B. N. Holben, M. D. King, Y. J. Kaufman, T. F. Eck, and I.
8 Slutsker: Accuracy assessment of aerosol optical properties retrieval from AERONET sun
9 and sky radiance measurements. *J. Geophys. Res.*, 105, 9791–9806, 2000.

10 Eckhardt, S., Quennehen, B., Olivié, D. J. L., Berntsen, T. K., Cherian, R., Christensen, J. H.,
11 Collins, W., Crepinsek, S., Daskalakis, N., Flanner, M., Herber, A., Heyes, C., Hodnebrog,
12 Ø., Huang, L., Kanakidou, M., Klimont, Z., Langner, J., Law, K. S., Massling, A.,
13 Myriokefalitakis, S., Nielsen, I. E., Nøjgaard, J. K., Quaas, J., Quinn, P. K., Raut, J.-C.,
14 Rumbold, S. T., Schulz, M., Skeie, R. B., Skov, H., Lund, M. T., Uttal, T., von Salzen, K.,
15 Mahmood, R., and Stohl, A.: Current model capabilities for simulating black carbon and
16 sulfate concentrations in the Arctic atmosphere: a multi-model evaluation using a
17 comprehensive measurement data set, *Atmos. Chem. Phys. Discuss.*, 15, 10425-10477,
18 doi:10.5194/acpd-15-10425-2015, 2015.

19 Edwards, J. and Slingo, A.: Studies with a flexible new radiation code. I: Choosing a
20 configuration for a large-scale model, *Q. J. Roy. Meteor. Soc.*, 122, 689–719, 1996.

21 Emmons, L. K., Walters, S., Hess, P. G., Lamarque, J.-F., Pfister, G. G., Fillmore, D.,
22 Granier, C., Guenther, A., Kinnison, D., Laepple, T., Orlando, J., Tie, X., Tyndall, G.,
23 Wiedinmyer, C., Baughcum, S. L., and Kloster, S.: Description and evaluation of the Model
24 for Ozone and Related chemical Tracers, version 4 (MOZART-4), *Geosci. Model Dev.*, 3, 43–
25 67, doi:10.5194/gmd-3-43-2010, 2010.

26 Fiore, A.M., Naik, V., and Leibensperger, E.M.: Air quality and climate connections, *J. Air*
27 *Waste Ma.*, 65:6, 645-685, doi:10.1080/10962247.2015.1040526, 2015.

28 Fry, M. M., et al.: The influence of ozone precursor emissions from four world regions on
29 tropospheric composition and radiative climate forcing, *J. Geophys. Res.*, 117, D07306,
30 doi:10.1029/2011JD017134, 2012.

1 Fujino, J., R. Nair, M. Kainuma, T. Masui, Y. Matsuoka: Multigas mitigation analysis on
2 stabilization scenarios using AIM global model. *The Energy Journal*, Special Issue 3, 343—
3 354, 2006.

4 Fuglestedt, Jan S., Keith P. Shine, Jolene Cook, Terje Berntsen, David S. Lee, Andrea
5 Stenke, Ragnhild Bieltvedt Skeie, Guus Velders and Ian Waitz: Transport Impacts on
6 Atmosphere and Climate: Metrics. *Atmospheric Environment*, 44, 4648-4677, 2010.

7 Gadhavi, H. S., Renuka, K., Ravi Kiran, V., Jayaraman, A., Stohl, A., Klimont, Z., and Beig,
8 G.: Evaluation of black carbon emission inventories using a Lagrangian dispersion model – a
9 case study over Southern India, *Atmos. Chem. Phys.*, 15, 1447–1461, doi:10.5194/acp-15-
10 1447-2015, 2015.

11 Ghan, S. J.: Technical Note: Estimating aerosol effects on cloud radiative forcing, *Atmos.*
12 *Chem. Phys.*, 13, 9971-9974, doi:10.5194/acp-13-9971-2013, 2013.

13 Hauglustaine, D. A., Balkanski, Y., and Schulz, M.: A global model simulation of present and
14 future nitrate aerosols and their direct radiative forcing of climate, *Atmos. Chem. Phys.*, 14,
15 11031-11063, doi:10.5194/acp-14-11031-2014, 2014.

16 Hegg, D. A.: Cloud condensation nucleus-sulphate mass relationship and cloud albedo, *J.*
17 *Geophys. Res.*, 99(D12), 25903–25907, doi:10.1029/94JD02224, 1994.

18 Hewitt, H. T., Copsey, D., Culverwell, I. D., Harris, C. M., Hill, R. S. R., Keen, A. B.,
19 McLaren, A. J., and Hunke, E. C.: Design and implementation of the infrastructure of
20 HadGEM3: the next-generation Met Office climate modelling system, *Geosci. Model Dev.*, 4,
21 223–253, doi:10.5194/gmd-4-223-2011, 2011.

22 Hodnebrog, Ø, G. Myhre, and B.H. Samset. How shorter black carbon lifetime alters its
23 climate effect. *Nature Communications*, 5, 5065, doi:10.1038/ncomms6065, 2014.

24 Holmes, C. D., M.J. Prather, O.A. Søvde, and G. Myhre: Future methane, hydroxyl, and their
25 uncertainties: key climate and emission parameters for future predictions, *Atmos. Chem.*
26 *Phys.*, 13, 285-302, doi:10.5194/acp-13-285-2013, 2013.

27 Iacono, M. J., J. S. Delamere, E. J. Mlawer, M. W. Shephard, S. A. Clough, and W. D.
28 Collins: Radiative forcing by long-lived greenhouse gases: Calculations with the AER
29 radiative transfer models, *J. Geophys. Res.*, 113, D13103, doi:10.1029/2008JD009944, 2008.

1 Iversen, T., Bentsen, M., Bethke, I., Debernard, J. B., Kirkevåg, A., Seland, Ø., Drange, H.,
2 Kristjansson, J. E., Medhaug, I., Sand, M., and Seierstad, I. A.: The Norwegian Earth System
3 Model, NorESM1-M – Part 2: Climate response and scenario projections, *Geosci. Model*
4 *Dev.*, 6, 389–415, doi:10.5194/gmd-6-389-2013, 2013.

5 Jiang, J. H., et al.: Evaluation of cloud and water vapor simulations in CMIP5 climate models
6 using NASA “A-Train” satellite observations, *J. Geophys. Res.*, 117, D14105,
7 doi:10.1029/2011JD017237, 2012.

8 Jiao, C., Flanner, M. G., Balkanski, Y., Bauer, S. E., Bellouin, N., Berntsen, T. K., Bian, H.,
9 Carslaw, K. S., Chin, M., De Luca, N., Diehl, T., Ghan, S. J., Iversen, T., Kirkevåg, A., Koch,
10 D., Liu, X., Mann, G. W., Penner, J. E., Pitari, G., Schulz, M., Seland, Ø., Skeie, R. B.,
11 Steenrod, S. D., Stier, P., Takemura, T., Tsigaridis, K., van Noije, T., Yun, Y., and Zhang, K.:
12 An AeroCom assessment of black carbon in Arctic snow and sea ice, *Atmos. Chem. Phys.*,
13 14, 2399-2417, doi:10.5194/acp-14-2399-2014, 2014.

14 Jones, A., Roberts, D. L., and Slingo, A. A climate model study of indirect radiative forcing
15 by anthropogenic sulphate aerosols. *Nature*, 370, 450–453, 1994.

16 Kirkevåg, A., Iversen, T., Seland, Ø., Hoose, C., Kristjánsson, J. E., Struthers, H., Ekman, A.
17 M. L., Ghan, S., Griesfeller, J., Nilsson, E. D., and Schulz, M.: Aerosol–climate interactions
18 in the Norwegian Earth System Model – NorESM1-M, *Geosci. Model Dev.*, 6, 207–244,
19 doi:10.5194/gmd-6-207-2013, 2013.

20 Koch, D. and Del Genio, A. D.: Black carbon semi-direct effects on cloud cover: review and
21 synthesis, *Atmos. Chem. Phys.*, 10, 7685-7696, doi:10.5194/acp-10-7685-2010, 2010.

22 Koffi, B., Schulz, M., Breon, F.M., Dentener, F., Steensen, B. M., Griesfeller, J., Winker, D.,
23 Balkanski, Y., Bauer, S.E., Bellouin, N., Berntsen, T., Bian, H.S., Chin, M., Diehl, T., Easter,
24 R., Ghan, S., Hauglustaine, D.A., Iversen, T., Kirkevåg, A., Liu, X.H., Lohmann, U., Myhre,
25 G., Rasch, P., Seland, O., Skeie, R.B., Steenrod, S.D., Stier, P., Tackett, J., Takemura, T.,
26 Tsigaridis, K., Vuolo, M.R., Yoon, J., Zhang, K.: Evaluation of the aerosol vertical
27 distribution in global aerosol models through comparison against CALIOP measurements:
28 AeroCom phase II results. *J. Geophys. Res.*, 121 (12), 7254-7283,
29 doi:10.1002/2015JD024639, 2016.

1 Kooperman, G. J., M. S. Pritchard, S. J. Ghan, M. Wang, R. C. J. Somerville, and L. M.
2 Russell: Constraining the influence of natural variability to improve estimates of global
3 aerosol indirect effects in a nudged version of the Community Atmosphere Model 5,
4 *J. Geophys. Res.*, 117, D23204, doi:10.1029/2012JD018588, 2012.

5 Kristiansen, N.I., Stohl, A., and Wotawa, G.: Atmospheric removal times of the aerosol-
6 bound radionuclides ^{137}Cs and ^{131}I measured after the Fukushima Dai-ichi nuclear accident –
7 a constraint for air quality and climate models, *Atmos. Chem. Phys.*, 12, 10759–10769,
8 doi:10.5194/acp-12-10759-2012, 2012.

9 Kristiansen, N. I., Stohl, A., Oliv  , D. J. L., Croft, B., S  vde, O. A., Klein, H., Christoudias,
10 T., Kunkel, D., Leadbetter, S. J., Lee, Y. H., Zhang, K., Tsigaridis, K., Bergman, T.,
11 Evangeliou, N., Wang, H., Ma, P.-L., Easter, R. C., Rasch, P. J., Liu, X., Pitari, G., Di
12 Genova, G., Zhao, S. Y., Balkanski, Y., Bauer, S. E., Faluvegi, G. S., Kokkola, H., Martin, R.
13 V., Pierce, J. R., Schulz, M., Shindell, D., Tost, H., and Zhang, H.: Evaluation of observed
14 and modelled aerosol lifetimes using radioactive tracers of opportunity and an ensemble of 19
15 global models, *Atmos. Chem. Phys.*, 16, 3525–3561, doi:10.5194/acp-16-3525-2016, 2016.

16 Lacis, A.A., D.J. Wuebbles, and J.A. Logan: Radiative forcing of climate by changes in the
17 vertical distribution of ozone, *J. Geophys. Res.*, 95, 9971–9981,
18 doi:10.1029/JD095iD07p09971, 1990.

19 Lin, X., Trainer, M., and Liu, S. C.: On the nonlinearity of the tropospheric ozone production,
20 *J. Geophys. Res.*, 93(D12), 15879–15888, doi:10.1029/JD093iD12p15879, 1988.

21 Lohmann, U., Stier, P., Hoose, C., Ferrachat, S., Kloster, S., Roeckner, E., and Zhang, J.:
22 Cloud microphysics and aerosol indirect effects in the global climate model ECHAM5-HAM,
23 *Atmos. Chem. Phys.*, 7, 3425–3446, doi:10.5194/acp-7-3425-2007, 2007.

24 Mann, G. W., Carslaw, K. S., Spracklen, D. V., Ridley, D. A., Manktelow, P. T.,
25 Chipperfield, M. P., Pickering, S. J., and Johnson, C. E.: Description and evaluation of
26 GLOMAP-mode: a modal global aerosol microphysics model for the UKCA composition-
27 climate model, *Geosci. Model Dev.*, 3, 519–551, doi:10.5194/gmd-3-519-2010, 2010.

28 Metzger, S., F. Dentener, S. Pandis, and J. Lelieveld, Gas/aerosol partitioning, 1, A
29 computationally efficient model, *J. Geophys. Res.*, 107, D16, doi:10.1029/2001JD001102,
30 2002.

1 Myhre, G., E.J. Highwood, K.P. Shine, and F. Stordal: New estimates of radiative forcing due
2 to well mixed greenhouse gases, *Geophys. Res. Lett.*, 25, 14, 2715-2718,
3 doi:10.1029/98GL01908, 1998.

4 Myhre, G., Karlsdottir, S., Isaksen, I. S. A., and Stordal, F.: Radiative forcing due to changes
5 in tropospheric ozone in the period 1980 to 1996, *J. Geophys. Res.*, 105, 28935–28942, 2000.

6 Myhre, G., Bellouin, N., Berglen, T. F., Berntsen, T. K., Boucher, O., Grini, A., Isaksen, I. S.
7 A., Johnsrud, M., Mishchenko, M. I., Stordal, F., and Tanre, D.: Comparison of the radiative
8 properties and direct radiative effect of aerosols from a global aerosol model and remote
9 sensing data over ocean, *Tellus B*, 59, 115–129, 2007a.

10 Myhre, G., J. S. Nilsen, L. Gulstad, K. P. Shine, B. Rognerud, and I. S. A. Isaksen, Radiative
11 forcing due to stratospheric water vapour from CH₄ oxidation, *Geophys. Res. Lett.*, 34,
12 L01807, doi:10.1029/2006GL027472, 2007b.

13 Myhre, G., Berglen, T. F., Johnsrud, M., Hoyle, C. R., Berntsen, T. K., Christopher, S. A.,
14 Fahey, D. W., Isaksen, I. S. A., Jones, T. A., Kahn, R. A., Loeb, N., Quinn, P., Remer, L.,
15 Schwarz, J. P., and Yttri, K. E.: Modelled radiative forcing of the direct aerosol effect with
16 multi-observation evaluation, *Atmos. Chem. Phys.*, 9, 4, 1365-1392, 10.5194/acp-9-1365-
17 2009, 2009.

18 Myhre, G., D. Shindell, F.-M. Bréon, W. Collins, J. Fuglestedt, J. Huang, D. Koch, J.-F.
19 Lamarque, D. Lee, B. Mendoza, T. Nakajima, A. Robock, G. Stephens, T. Takemura and H.
20 Zhang: Anthropogenic and Natural Radiative Forcing. In: *Climate Change 2013: The Physical
21 Science Basis. Contribution of Working Group I to the Fifth Assessment Report of the
22 Intergovernmental Panel on Climate Change* [Stocker, T.F., D. Qin, G.-K. Plattner, M.
23 Tignor, S.K. Allen, J. Boschung, A. Nauels, Y. Xia, V. Bex and P.M. Midgley (eds.)].
24 Cambridge University Press, Cambridge, United Kingdom and New York, NY, USA, 2013a.

25 Myhre, G., B.H. Samset, M. Schulz, Y. Balkanski, S. Bauer, T.K. Berntsen, H. Bian, N.
26 Bellouin, M. Chin, T. Diehl, R.C. Easter, J. Feichter, S.J. Ghan, D. Hauglustaine, T. Iversen,
27 S. Kinne, A. Kirkevåg, J.-F. Lamarque, G. Lin, X. Liu, M.T. Lund, G. Luo, X. Ma, T. van
28 Noije, J. E. Penner, P.J. Rasch, A. Ruiz, Ø. Seland, R.B. Skeie, P. Stier, T. Takemura, K.
29 Tsigaridis, P. Wang, Z. Wang, L. Xu, H. Yu, F. Yu, J.-H. Yoon, K. Zhang, H. Zhang, and C.

1 Zhou.: Radiative forcing of the direct aerosol effect from AeroCom Phase II simulations.
2 *Atmos. Chem. Phys.*, 13, 1853-1877, doi:10.5194/acp-13-1853-2013, 2013b.

3 Neale, R.B., *et al.*, Description of the NCAR Community Atmosphere Model (CAM 4.0),
4 NCAR Technical Report, NCAR/TN-485+STR, National Center for Atmospheric Research
5 (NCAR), Boulder, Colorado, 2010.

6 O'Connor, F. M., Johnson, C. E., Morgenstern, O., Abraham, N. L., Braesicke, P., Dalvi, M.,
7 Folberth, G. A., Sanderson, M. G., Telford, P. J., Voulgarakis, A., Young, P. J., Zeng, G.,
8 Collins, W. J., and Pyle, J. A.: Evaluation of the new UKCA climate-composition model –
9 Part 2: The Troposphere, *Geosci. Model Dev.*, 7, 41–91, doi:10.5194/gmd-7-41-2014, 2014.

10 Pan, X., Chin, M., Gautam, R., Bian, H., Kim, D., Colarco, P. R., Diehl, T. L., Takemura, T.,
11 Pozzoli, L., Tsigaridis, K., Bauer, S., and Bellouin, N.: A multi-model evaluation of aerosols
12 over South Asia: common problems and possible causes, *Atmos. Chem. Phys.*, 15, 5903-5928,
13 doi:10.5194/acp-15-5903-2015, 2015.

14 Paoli, R., Cariolle, D., and Sausen, R.: Review of effective emissions modeling and
15 computation, *Geosci. Model Dev.*, 4, 643–667, doi:10.5194/gmd-4-643-2011, 2011.

16 Prather, M.J. Time scales in atmospheric chemistry: Theory, GWPs for CH₄ and CO, and
17 runaway growth, *Geophys. Res. Lett.*, 23, 19, 2597—2600, doi:10.1029/96GL02371, 1996.

18 Quaas, J., Y. Ming, S. Menon, T. Takemura, M. Wang, J.E. Penner, A. Gettelman, U.
19 Lohmann, N. Bellouin, O. Boucher, A.M. Sayer, G.E. Thomas, A. McComiskey, G. Feingold,
20 C. Hoose, J.E. Kristjansson, X. Liu, Y. Balkanski, L.J. Donner, P.A. Ginoux, P. Stier, B.
21 Grandey, J. Feichter, I. Sednev, S.E. Bauer, D. Koch, R.G. Grainger, A. Kirkevåg, T. Iversen,
22 Ø. Seland, R. Easter, S.J. Ghan, P.J. Rasch, H. Morrison, J.-F. Lamarque, M.J. Iacono, S.
23 Kinne, and M. Schulz. Aerosol indirect effects - general circulation model intercomparison
24 and evaluation with satellite data. *Atmos. Chem. Phys.*, 9, 8697-8717, 2009.

25 Quennehen, B., Raut, J.-C., Law, K. S., Daskalakis, N., Ancellet, G., Clerbaux, C., Kim, S.-
26 W., Lund, M. T., Myhre, G., Olivié, D. J. L., Safieddine, S., Skeie, R. B., Thomas, J. L.,
27 Tsyro, S., Bazureau, A., Bellouin, N., Hu, M., Kanakidou, M., Klimont, Z., Kupiainen, K.,
28 Myriokefalitakis, S., Quaas, J., Rumbold, S. T., Schulz, M., Cherian, R., Shimizu, A., Wang,
29 J., Yoon, S.-C., and Zhu, T.: Multi-model evaluation of short-lived pollutant distributions

1 over east Asia during summer 2008, *Atmos. Chem. Phys.*, 16, 10765-10792, doi:10.5194/acp-
2 16-10765-2016, 2016.

3 Randles, C. A., Kinne, S., Myhre, G., Schulz, M., Stier, P., Fischer, J., Doppler, L.,
4 Highwood, E., Ryder, C., Harris, B., Huttunen, J., Ma, Y., Pinker, R. T., Mayer, B.,
5 Neubauer, D., Hitzenberger, R., Oreopoulos, L., Lee, D., Pitari, G., Di Genova, G., Quaas, J.,
6 Rose, F. G., Kato, S., Rumbold, S. T., Vardavas, I., Hatzianastassiou, N., Matsoukas, C.,
7 Yu, H., Zhang, F., Zhang, H., and Lu, P.: Intercomparison of shortwave radiative transfer
8 schemes in global aerosol modeling: results from the AeroCom Radiative Transfer
9 Experiment, *Atmos. Chem. Phys.*, 13, 2347–2379, doi:10.5194/acp-13-2347-2013, 2013.

10 Riahi, K., Gruebler, A., and Nakicenovic, N.: Scenarios of long-term socio-economic and
11 environmental development under climate stabilization, *Technol. Forecast. Soc. Change*, 74,
12 887–935, 2007.

13 Saleh, R., Robinson, E.S., Tkacik, D.S., Ahern, A.T., Liu, S., Aiken, A.C., Sullivan, R.C.,
14 Presto, A.A., Dubey, M.K., Yokelson, R.J., Donahue, N.M., Robinson, A.L.: Brownness of
15 organics in aerosols from biomass burning linked to their black carbon content, *Nature*
16 *Geoscience*, 7, 647–650, doi:10.1038/ngeo2220, 2014.

17 Samset, B.H., G. Myhre, M. Schulz, Y. Balkanski, S. Bauer, T.K. Berntsen, H. Bian, N.
18 Bellouin, T. Diehl, R.C. Easter, S.J. Ghan, T. Iversen, S. Kinne, A. Kirkevåg, J.-F. Lamarque,
19 G. Lin, X. Liu, J.E. Penner, Ø. Seland, R.B. Skeie, P. Stier, T. Takemura, K. Tsigaridis, and
20 K. Zhang. Black carbon vertical profiles strongly affect its radiative forcing uncertainty.
21 *Atmos. Chem. Phys.*, 13, 2423-2434, doi:10.5194/acp-13-2423-2013, 2013.

22 Samset, B. H., Myhre, G., Herber, A., Kondo, Y., Li, S.-M., Moteki, N., Koike, M.,
23 Oshima, N., Schwarz, J. P., Balkanski, Y., Bauer, S. E., Bellouin, N., Berntsen, T. K.,
24 Bian, H., Chin, M., Diehl, T., Easter, R. C., Ghan, S. J., Iversen, T., Kirkevåg, A.,
25 Lamarque, J.-F., Lin, G., Liu, X., Penner, J. E., Schulz, M., Seland, Ø., Skeie, R. B., Stier, P.,
26 Takemura, T., Tsigaridis, K., and Zhang, K.: Modelled black carbon radiative forcing and
27 atmospheric lifetime in AeroCom Phase II constrained by aircraft observations, *Atmos. Chem.*
28 *Phys.*, 14, 12465-12477, doi:10.5194/acp-14-12465-2014, 2014.

29 Schmale, J., Shindell, D., von Schneidmesser, E., Chabay, I., and Lawrence, M.: Clean up
30 our skies, *Nature*, 515, 335–337, 2014.

1 Schulz, M., Olivié, D., Tsyro, S., Kanakidou, M., Myriokefalitakis, S., Daskalakis, N., Im, U.,
2 Fanourgakis, G., Hodnebrog, Ø., Skeie, R., Lund, M., Myhre, G., Bellouin, N., Rumbold, S.,
3 Collins, B., Cherian, R., and Quaas, J.: ECLIPSE Deliverable 2.1: Report on model accuracy,
4 available from <http://eclipse.nilu.no/language/en-GB/ProjectOverview/Deliverables.aspx>,
5 2015.

6 Shindell, D., and G. Faluvegi: Climate response to regional radiative forcing during the
7 twentieth century, *Nature Geosci.*, 2, 294-300, doi:10.1038/ngeo473, 2009.

8 Shindell, D.T., G. Faluvegi, D.M. Koch, G.A. Schmidt, N. Unger, and S.E. Bauer: Improved
9 attribution of climate forcing to emissions. *Science*, 326, 716-718,
10 doi:10.1126/science.1174760, 2009.

11 Shindell, D. T., Lamarque, J.-F., Schulz, M., Flanner, M., Jiao, C., Chin, M., Young, P. J.,
12 Lee, Y. H., Rotstayn, L., Mahowald, N., Milly, G., Faluvegi, G., Balkanski, Y., Collins, W. J.,
13 Conley, A. J., Dalsoren, S., Easter, R., Ghan, S., Horowitz, L., Liu, X., Myhre, G.,
14 Nagashima, T., Naik, V., Rumbold, S. T., Skeie, R., Sudo, K., Szopa, S., Takemura, T.,
15 Voulgarakis, A., Yoon, J.-H., and Lo, F.: Radiative forcing in the ACCMIP historical and
16 future climate simulations, *Atmos. Chem. Phys.*, 13, 2939-2974, doi:10.5194/acp-13-2939-
17 2013, 2013.

18 Shindell, D.: Inhomogeneous forcing and transient climate sensitivity. *Nature Climate*
19 *Change*, 4, 274–277, doi:10.1038/nclimate2136, 2014.

20 Shine, K.P., Fuglestedt, J.S., Hailemariam, K., and Stuber, S.: Alternatives to the global
21 warming potential for comparing climate impacts of emissions of greenhouse gases, *Climatic*
22 *Change*, 68, 3, 281—302, doi:10.1007/s10584-005-1146-9, 2005.

23 Skeie, R. B., Berntsen, T. K., Myhre, G., Tanaka, K., Kvalevåg, M. M., and Hoyle, C. R.:
24 Anthropogenic radiative forcing time series from pre-industrial times until 2010, *Atmos.*
25 *Chem. Phys.*, 11, 11827-11857, doi:10.5194/acp-11-11827-2011, 2011.

26 Smith, S.J., Karas, J., Edmonds, J., Eom, J., and Mizrahi, A.: Sensitivity of multi-gas climate
27 policy to emission metrics, *Climatic Change*, 117, 4, 663-675, doi:10.1007/s10584-012-0565-
28 7, 2013.

1 Stevens, B., and Feingold, G. Untangling aerosol effects on clouds and precipitation in a
2 buffered system, *Nature*, 461, 607-613, doi:10.1038/nature08281, 2009.

3 Stevens, B., Giorgetta, M., Esch, M., Mauritsen, T., Crueger, T., Rast, S., Salzmann, M.,
4 Schmidt, H., Bader, J., Block, K., Brokopf, R., Fast, I., Kinne, S., Kornblueh, L., Lohmann,
5 U., Pincus, R., Reichler, T., and Roeckner, E.: Atmospheric component of the MPI-M Earth
6 System Model: ECHAM6, *J. Adv. Model. Earth Sy.*, 5, 146–172, 2013.

7 Stevenson, D.S., P.J. Young, V. Naik, J.-F. Lamarque, D.T. Shindell, A. Voulgarakis, R.B.
8 Skeie, S.B. Dalsoren, G. Myhre, T.K. Berntsen, G.A. Folberth, S.T. Rumbold, W.J. Collins,
9 I.A. MacKenzie, R.M. Doherty, G. Zeng, T.P.C. van Noije, A. Strunk, D. Bergmann, P.
10 Cameron-Smith, D.A. Plummer, S.A. Strode, L. Horowitz, Y.H. Lee, S. Szopa, K. Sudo, T.
11 Nagashima, B. Josse, I. Cionni, M. Righi, V. Eyring, A. Conley, K.W. Bowman, and O. Wild:
12 Tropospheric ozone changes, radiative forcing and attribution to emissions in the
13 Atmospheric Chemistry and Climate Model Inter-comparison Project (ACCMIP). *Atmos.*
14 *Chem. Phys.*, **13**, 3063-3085, doi:10.5194/acp-13-3063-2013, 2013.

15 Stier, P., Feichter, J., Kinne, S., Kloster, S., Vignati, E., Wilson, J., Ganzeveld, L., Tegen, I.,
16 Werner, M., Balkanski, Y., Schulz, M., Boucher, O., Minikin, A., and Petzold, A.: The
17 aerosol-climate model ECHAM5-HAM, *Atmos. Chem. Phys.*, 5, 1125–1156, doi:10.5194/acp-
18 5-1125-2005, 2005.

19 Stier, P., N.A.J. Schutgens, N. Bellouin, H. Bian, O. Boucher, M. Chin, S. Ghan, N. Huneus,
20 S. Kinne, G. Lin, X. Ma, G. Myhre, J.E. Penner, C.A. Randles, B. Samset, M. Schulz, T.
21 Takemura, F. Yu, H. Yu, and C. Zhou. Host model uncertainties in aerosol radiative forcing
22 estimates: results from the AeroCom Prescribed intercomparison study. *Atmos. Chem. Phys.*,
23 13, 3245-3270, doi:10.5194/acp-13-3245-2013, 2013.

24 Stohl, A., Aamaas, B., Amann, M., Baker, L. H., Bellouin, N., Berntsen, T. K., Boucher, O.,
25 Cherian, R., Collins, W., Daskalakis, N., Dusinska, M., Eckhardt, S., Fuglestedt, J. S., Harju,
26 M., Heyes, C., Hodnebrog, Ø., Hao, J., Im, U., Kanakidou, M., Klimont, Z., Kupiainen, K.,
27 Law, K. S., Lund, M. T., Maas, R., MacIntosh, C. R., Myhre, G., Myriokefalitakis, S., Olivie,
28 D., Quaas, J., Quennehen, B., Raut, J.-C., Rumbold, S. T., Samset, B. H., Schulz, M., Seland,
29 Ø., Shine, K. P., Skeie, R. B., Wang, S., Yttri, K. E., and Zhu, T.: Evaluating the climate and

1 air quality impacts of short-lived pollutants, *Atmos. Chem. Phys. Discuss.*, 15, 15155-15241,
2 doi:10.5194/acpd-15-15155-2015, 2015.

3 Streets, D. G., et al.: An inventory of gaseous and primary aerosol emissions in Asia in the
4 year 2000. *J. Geophys. Res.*, 108, 8809, doi:10.1029/2002JD003093, D21, 2003.

5 Taylor, J.P. and A. McHaffie: Measurements of cloud susceptibility, *J. Atmos. Sci.*, 51, 10,
6 1298—1306, 1994.

7 Tsigaridis, K., Daskalakis, N., Kanakidou, M., Adams, P. J., Artaxo, P., Bahadur, R.,
8 Balkanski, Y., Bauer, S. E., Bellouin, N., Benedetti, A., Bergman, T., Berntsen, T. K.,
9 Beukes, J. P., Bian, H., Carslaw, K. S., Chin, M., Curci, G., Diehl, T., Easter, R. C., Ghan, S.
10 J., Gong, S. L., Hodzic, A., Hoyle, C. R., Iversen, T., Jathar, S., Jimenez, J. L., Kaiser, J. W.,
11 Kirkevåg, A., Koch, D., Kokkola, H., Lee, Y. H., Lin, G., Liu, X., Luo, G., Ma, X., Mann, G.
12 W., Mihalopoulos, N., Morcrette, J.-J., Müller, J.-F., Myhre, G., Myriokefalitakis, S., Ng, N.
13 L., O'Donnell, D., Penner, J. E., Pozzoli, L., Pringle, K. J., Russell, L. M., Schulz, M., Sciare,
14 J., Seland, Ø., Shindell, D. T., Sillman, S., Skeie, R. B., Spracklen, D., Stavrou, T.,
15 Steenrod, S. D., Takemura, T., Tiitta, P., Tilmes, S., Tost, H., van Noije, T., van Zyl, P. G.,
16 von Salzen, K., Yu, F., Wang, Z., Wang, Z., Zaveri, R. A., Zhang, H., Zhang, K., Zhang, Q.,
17 and Zhang, X.: The AeroCom evaluation and intercomparison of organic aerosol in global
18 models, *Atmos. Chem. Phys.*, 14, 10845-10895, doi:10.5194/acp-14-10845-2014, 2014.

19 Viana, M., Hammingh, P., Colette, A., Querol, X., Degraeuwe, B., de Vlieger, I., van
20 Aardenne, J.: Impact of maritime transport emissions on coastal air quality in Europe, *Atmos.*
21 *Environ.*, 90, 96—105, doi:10.1016/j.atmosenv.2014.03.046, 2014.

22 Vignati, E., Wilson, J., and Stier, P.: M7: an efficient size-resolved aerosol microphysics
23 module for large-scale aerosol transport models, *J. Geophys. Res.*, 109, D22202,
24 doi:10.1029/2003JD004485, 2004.

25 von Schneidemesser, E. *et al.*: Chemistry and the linkages between air quality and climate
26 change, *Chem. Rev.*, 115, 3856–97, 2015.

27 Voulgarakis, A., Naik, V., Lamarque, J.-F., Shindell, D. T., Young, P. J., Prather, M. J., Wild,
28 O., Field, R. D., Bergmann, D., Cameron-Smith, P., Cionni, I., Collins, W. J., Dalsøren, S. B.,
29 Doherty, R. M., Eyring, V., Faluvegi, G., Folberth, G. A., Horowitz, L. W., Josse, B.,
30 MacKenzie, I. A., Nagashima, T., Plummer, D. A., Righi, M., Rumbold, S. T., Stevenson, D.

1 S., Strode, S. A., Sudo, K., Szopa, S., and Zeng, G.: Analysis of present day and future OH
2 and methane lifetime in the ACCMIP simulations, *Atmos. Chem. Phys.*, 13, 2563-2587,
3 doi:10.5194/acp-13-2563-2013, 2013.

4 Wang, X., Heald, C. L., Ridley, D. A., Schwarz, J. P., Spackman, J. R., Perring, A. E.,
5 Coe, H., Liu, D., and Clarke, A. D.: Exploiting simultaneous observational constraints on
6 mass and absorption to estimate the global direct radiative forcing of black carbon and brown
7 carbon, *Atmos. Chem. Phys.*, 14, 10989-11010, doi:10.5194/acp-14-10989-2014, 2014a.

8 Wang, Q. Q., D.J. Jacob, J.R. Spackman, A.R. Perring, J.P. Schwartz, N. Moteki, E.A.
9 Marais, C. Ge, J. Wang, and S.R.H. Barrett: Global budget and radiative forcing of black
10 carbon aerosol: Constraints from pole-to-pole (HIPPO) observations across the Pacific, *J.*
11 *Geophys. Res.*, 119, 195–206, doi:10.1002/2013JD020824, 2014b.

12 Wang, R., Y. Balkanski, O. Boucher, P. Ciais, G. L. Schuster, F. Chevallier, B. H. Samset, J.
13 Liu, S. Piao, M. Valari, S. Tao, Quantifying the role of black carbon in the Earth's climate
14 system, *Nature Scientific Reports*, submitted, 2015.

15 Wilcox, E. M.: Stratocumulus cloud thickening beneath layers of absorbing smoke aerosol,
16 *Atmos. Chem. Phys.*, 10, 11769-11777, doi:10.5194/acp-10-11769-2010, 2010.

17 Wilcox, L. J., Highwood, E. J., Booth, B. B. B. and Carslaw, K. S.: Quantifying sources of
18 inter-model diversity in the cloud albedo effect. *Geophys. Res. Lett.*, 42: 1568–1575. doi:
19 10.1002/2015GL063301, 2015.

20 WMO: Scientific Assessment of Ozone Depletion: 2014, Global Ozone Research and
21 Monitoring Project - Report No. 55, World Meteorological Organization, Geneva,
22 Switzerland, 2014.

23 Young, P. J., Archibald, A. T., Bowman, K. W., Lamarque, J.-F., Naik, V., Stevenson, D. S.,
24 Tilmes, S., Voulgarakis, A., Wild, O., Bergmann, D., Cameron-Smith, P., Cionni, I., Collins,
25 W. J., Dalsøren, S. B., Doherty, R. M., Eyring, V., Faluvegi, G., Horowitz, L. W., Josse, B.,
26 Lee, Y. H., MacKenzie, I. A., Nagashima, T., Plummer, D. A., Righi, M., Rumbold, S. T.,
27 Skeie, R. B., Shindell, D. T., Strode, S. A., Sudo, K., Szopa, S., and Zeng, G.: Pre-industrial
28 to end 21st century projections of tropospheric ozone from the Atmospheric Chemistry and
29 Climate Model Intercomparison Project (ACCMIP), *Atmos. Chem. Phys.*, 13, 2063-2090,
30 doi:10.5194/acp-13-2063-2013, 2013.

1 Yu, H., M. Chin, J.J West, C.S. Atherton, N. Bellouin, D. Bergmann, I. Bey, H. Bian, T.
2 Diehl, G. Forberth, P. Hess, M. Schulz, D. Shindell, T. Takemura, and Q. Tan. A multimodel
3 assessment of the influence of regional anthropogenic emission reductions on aerosol direct
4 radiative forcing and the role of intercontinental transport. *J. Geophys. Res.*, 118, 700-720,
5 doi:10.1029/2012JD018148, 2013.

6 Zhang, K., O'Donnell, D., Kazil, J., Stier, P., Kinne, S., Lohmann, U., Ferrachat, S., Croft, B.,
7 Quaas, J., Wan, H., Rast, S., and Feichter, J.: The global aerosol-climate model ECHAM-
8 HAM, version 2: sensitivity to improvements in process representations, *Atmos. Chem. Phys.*,
9 12, 8911–8949, doi:10.5194/acp-12-8911-2012, 2012.

10

6 Tables

Table 1. Specific radiative forcing (SRF), in $\text{mWm}^{-2} (\text{Tg y}^{-1})^{-1}$, of near-term climate forcers, as estimated by scientific assessments and multi-model inter-comparisons. Numbers shown are median and full range for all studies, except for: - Bond et al. (2013), where best estimate and 90% confidence range are given; - Yu et al. (2013), where mean and standard deviation are given; - Fry et al. (2012) where only the best estimate is available; - this study, where average and full range are given. Black Carbon (BC) and Organic Carbon (OC) aerosols are for fossil- and bio-fuel sources only, except for Bond et al. (2013) which also includes biomass-burning sources. For aerosols, the radiative forcing is for aerosol-radiation interactions (ari) only, except for the estimate by Bond et al. (2013) denoted “All”, which also includes aerosol-cloud and aerosol-surface interactions, and for estimates by this study, which also include aerosol-cloud interactions (aci).

Emitted compound	Climate Forcer	Reference	Method	SRF ($\text{mW m}^{-2} (\text{Tg yr}^{-1})^{-1}$)
SO ₂	SO ₄	Myhre et al. (2013b)	AeroCom, 15 models, ari only	-3.5 (-5.5 to -1.5)
		Shindell et al. (2013)	ACCMIP, 9 models, ari only	-4.3 (-6.4 to -2.0)
		Yu et al. (2013)	HTAP, 8 models, 4 source regions, ari only	-2.9 ± 0.8 to -3.9 ± 0.8 depending on region
		<i>This study</i>	ECLIPSE, 3 models, 3 source regions, 2 seasons, ari +aci	-3.1 to -10.7 (-1.9 to -17.7) depending on region
OC	OC	Myhre et al. (2013b)	AeroCom, 15 models, ari only	-3.8 (-7.6 to -1.3)
		Shindell et al. (2013)	ACCMIP, 4 models, ari only	-3.8 (-10.1 to -1.3)
		Yu et al. (2013)	HTAP, 8 models, 4 source regions, ari only	-3.7 ± 1.8 to -4.4 ± 1.7 depending on region
		<i>This study</i>	ECLIPSE, 3 models, 3 source regions, 2 seasons, ari +aci	-4.4 to -22.5 (+1.2 to -32.5) depending on region
BC	BC	Bond et al. (2013)	Assessment of models with observational constraints, ari	+51.1 (+6.5 to +181.8)

			only	
		Bond et al. (2013)	Assessment of models with observational constraints, all RF mechanisms	+746.3 (+12.3 to +344.3)
		Myhre et al. (2013b)	AeroCom, 15 models, ari only	+45.3 (+15.1 to +75.6)
		Shindell et al. (2013)	ACCMIP, 5 models, ari only	+50.4 (+35.3 to +95.7)
		Yu et al. (2013)	HTAP, 8 models, 4 source regions, ari only	+25.3±14.6 to +37.4±19.3 depending on region
		<i>This study</i>	ECLIPSE, 4 models, 3 source regions, 2 seasons, ari+aci+deposition on snow and rapid adjustments from the semi-direct effect	+28.7 to +69.7 (+9.8 to +101.1) depending on region
NH ₃	NO ₃	Myhre et al. (2013b)	AeroCom, 5 models, ari only	-3.9 (-13.3 to -1.0)
		<i>This study</i>	ECLIPSE, 1 model, 3 source regions, 2 seasons, ari+aci	-0.5 to -1.4 depending on region
CH ₄	CH ₄	Stevenson et al. (2013)	ACCMIP, 6 models	+2.2 (+1.8 to +3.0)
		<i>This study</i>	ECLIPSE, 3 models, 3 source regions	+1.5 (+1.2 to +2.0)
	O ₃	Stevenson et al. (2013)	ACCMIP, 6 models	+0.7 (+0.5 to +1.0)
		<i>This study</i>	ECLIPSE, 3 models, 3 source regions	+0.5 (+0.4 to +0.7)
NO _x	CH ₄	Fry et al. (2012)	HTAP, 11 models, 4 sources regions	-1.8 to -5.0 depending on region
		Stevenson et al. (2013)	ACCMIP, 6 models	-5.5 (-7.4 to -4.2)
		<i>This study</i>	ECLIPSE, 3 models, , 3 source regions, includes primary-mode O ₃	-0.4 to -2.1 (-2.6 to -2.5) depending on region
	O ₃	Fry et al. (2012)	HTAP, 11 models, 4 sources regions	+0.8 to +3.9 depending on region
		Stevenson et al. (2013)	ACCMIP, 6 models	+1.9 (+1.7 to +3.3)

		<i>This study</i>	ECLIPSE, 3 models, 3 source regions	+0.1 to +1.4 (+0.1 to +1.5) depending on region
	Aerosols	Fry et al. (2012)	HTAP, 11 models, 4 source regions, sulphate ari only	-0.5 to +0.2 depending on region
		<i>This study</i>	ECLIPSE, 3 models, , 3 source regions, ari+aci	-0.3 to -0.8 (-1.2 to +0.2) depending on region
CO	CH ₄	Fry et al. (2012)	HTAP, 11 models, 4 source regions	+0.08 to +0.10 depending on region
		Stevenson et al. (2013)	ACCMIP, 6 models	+0.11 (+0.07 to +0.13)
		<i>This study</i>	ECLIPSE, 3 models, , 3 source regions, includes primary-mode O ₃	+0.12 to +0.15 (+0.08 to +0.20) depending on region
	O ₃	Fry et al. (2012)	HTAP, 11 models, 4 source regions	+0.05 to +0.08 depending on region
		Stevenson et al. (2013)	ACCMIP, 6 models	+0.11 (+0.08 to 0.14)
		<i>This study</i>	ECLIPSE, 3 models, 3 source regions	+0.03 to +0.06 (+0.03 to +0.07) depending on region
	Aerosols	Fry et al. (2012)	HTAP, 11 models, 4 source regions, sulphate ari only	-0.005 to -0.01 depending on region
		<i>This study</i>	ECLIPSE, 3 models, , 3 source regions, ari+aci	+0.02 to +0.05 (-0.01 to +0.12) depending on region
	NMVOC	CH ₄	Fry et al. (2012)	HTAP, 11 models, 4 source regions
Stevenson et al. (2013)			ACCMIP, 6 models	+0.27 (+0.00 to +0.41)
<i>This study</i>			ECLIPSE, 3 models, , 3 source regions, includes primary-mode O ₃	+0.35 to +0.66 (+0.02 to +0.93) depending on region
O ₃		Fry et al. (2012)	HTAP, 11 models, 4 source regions	+0.2 to +0.4 depending on region
		Stevenson et al. (2013)	ACCMIP, 6 models	+0.34 (+0.21 to +0.39)

		<i>This study</i>	ECLIPSE, 3 models, 3 source regions	+0.63 to +1.15 (+0.31 to +1.48) depending on region
	Aerosols	Fry et al. (2012)	HTAP, 11 models, 4 source regions, sulphate ari only	-0.1 to 0 depending on region
		<i>This study</i>	ECLIPSE, 3 models, , 3 source regions, ari+aci	-0.18 to -0.74 (-1.48 to +0.86) depending on region

1

1 **Table 2.** List of models participating in the ECLIPSE radiative forcing simulations. Models
2 are either general circulation models (GCM) or chemistry-transport models (CTM).
3 Resolution indicates the horizontal resolution, in degrees, and the number of vertical levels.
4 Crosses indicate which aerosol species are represented in each model, among sulphate (SO₄),
5 black carbon (BC), organic carbon (OC), secondary organic aerosol (SOA), and nitrate
6 (NO₃) aerosols. Chemistry indicates whether the model includes an interactive tropospheric
7 ozone chemistry scheme. Radiation indicates whether radiation calculations are done
8 interactively (online) or offline from monthly distributions. Note that ozone radiative forcing
9 calculations are done offline for all models.

Model	Type	Resolution	SO ₄	BC	OC	SOA	NO ₃	Chemistry	Radiation
ECHAM6- HAM2	GCM	1.8°x1.8° L31	X	X	X				Online
HadGEM3- GLOMAP	GCM	1.8°x1.2° L38	X	X	X	X		X	Online
NorESM1- M	GCM	1.9°x2.5° L26	X	X	X	X		X	Online
OsloCTM2	CTM	2.8°x2.8° L60	X	X	X	X	X	X	Offline

10

1 **Table 3.** List of simulations made to provide radiative forcing by regional and seasonal
2 perturbations, and size of the emission perturbation applied to the anthropogenic component
3 for the year 2008, in $Tg\ yr^{-1}$. For some ozone precursors, HadGEM3 also perturbed the
4 biomass-burning component so the size of its perturbation is given in bracket (H:) for species
5 and regions with strong biomass-burning sources. Emitted masses are in [C] for black and
6 organic carbon, and volatile organic compounds. They are in [NO₂] for NO_x.

#	Perturbation applied	Emission perturbation ($Tg\ yr^{-1}$)	
		May—Oct	Nov—Apr
1	None (control simulation)		
2	SO ₂ emissions reduced by 20% in Europe	-0.77	-0.85
3	SO ₂ emissions reduced by 20% in East Asia	-3.14	-3.35
4	SO ₂ emissions reduced by 20% outside Europe, East Asia, and shipping sector	-5.1	-5.2
5	BC emissions reduced by 20% in Europe	-0.03	-0.05
6	BC emissions reduced by 20% in East Asia	-0.11	-0.18
7	BC emissions reduced by 20% outside Europe, East Asia, and shipping sector	-0.35	-0.36
8	OC emissions reduced by 20% in Europe	-0.04	-0.07
9	OC emissions reduced by 20% in East Asia	-0.21	-0.37
10	OC emissions reduced by 20% outside Europe, East Asia, and shipping sector	-0.80	-0.83
11	NH ₃ emissions reduced by 20% in Europe	-0.39	-0.39
12	NH ₃ emissions reduced by 20% in East Asia	-1.37	-1.35
13	NH ₃ emissions reduced by 20% outside Europe, East Asia, and shipping sector	-3.48	-3.43

14	NO _x emissions reduced by 20% in Europe	-1.00	-1.06
15	NO _x emissions reduced by 20% in East Asia	-2.03	-2.11
16	NO _x emissions reduced by 20% outside Europe, East Asia, and shipping sector	-6.27 (H: -7.17)	-6.37 (H: -6.69)
17	VOC emissions reduced by 20% in Europe	-0.06 to - 0.28	-0.07 to - 0.36
18	VOC emissions reduced by 20% in East Asia	-0.15 to - 0.55	-0.19 to - 0.84
19	VOC emissions reduced by 20% outside Europe, East Asia, and shipping sector	-0.15 to - 4.08	-0.19 to - 4.17
20	CO emissions reduced by 20% in Europe	-2.43	-3.09
21	CO emissions reduced by 20% in East Asia	-12.82 (H: -12.91)	-16.99 (H: -17.58)
22	CO emissions reduced by 20% outside Europe, East Asia, and shipping sector	-35.65 (H: -64.39)	-35.10 (H: -51.40)
23	All species of the shipping sector reduced by 20%	See Table 4.	
24	CH ₄ perturbations equivalent to global 20% emission reduction	See ΔE in Table 7.	

1

1 **Table 4.** *Size of the emission perturbation applied to the shipping sector for the year 2008, in*
 2 *Tg yr⁻¹. Emitted masses are in [C] for black and organic carbon, and volatile organic*
 3 *compounds. They are in [NO₂] for NO_x. Emissions used in ECHAM6 and NorESM1 are*
 4 *denoted with E and N, where different.*

Species	Emission perturbation (Tg yr ⁻¹)	
	May—Oct	Nov—Apr
SO ₂	-1.04 (E: -1.25)	-1.04 (E: -1.24)
BC	-0.01 (E: -0.02)	-0.01 (E: -0.02)
OC	-0.01 (E: -0.02)	-0.01 (E: -0.02)
NO _x	-1.70 (N: -1.10)	-1.67 (N: -1.10)
VOC	-0.04 to -0.21	-0.04 to -0.21
CO	-0.11	-0.11

5
6

1 **Table 5.** *Simulated lifetime, in days, of aerosol species and tropospheric ozone in the four*
2 *participating models.*

Species	ECHAM6	HadGEM3	NorESM1	OsloCTM2
Sulphate	4.0	5.2	4.2	3.5
BC	5.2	5.7	8.0	6.2
OC	5.0	6.6	7.7	5.0
Tropospheric ozone	n/a	20.7	26.4	Not diagnosed

3
4

1 **Table 6.** *Semi-direct radiative forcing (SDRF) by regional and seasonal perturbations of*
 2 *black carbon aerosols. Column 3 gives the scaling factor imposed to let rapid adjustments*
 3 *from the semi-direct effect emerge from natural variability. Column 4 gives the corresponding*
 4 *specific SDRF, in $mW m^{-2} (Tg[C] yr^{-1})^{-1}$, and its standard deviation over the 30 years.*
 5

Region	Season	Scaling factor	Specific SDRF
Europe	Summer	500	-31 ± 13
	Winter	500	-3 ± 8
East Asia	Summer	150	-38 ± 12
	Winter	150	$+1 \pm 7$
Global	Summer	30	-40 ± 18
	Winter	30	-14 ± 11

6
7

1 **Table 7.** Characteristics of the methane budget in ECLIPSE models. For NorESM1, numbers
2 are given for the Summer perturbation simulation. From left to right, columns give: methane
3 lifetime to destruction by OH, τ_{OH} in years, for the control (Ctl) and perturbed (Per)
4 simulations; total methane lifetime, τ_{tot} in years, in Ctl and Per simulations; total methane
5 burden, B in Tg[CH₄], in Ctl and Per simulations; methane feedback factor f ; equivalent
6 methane emission perturbation, ΔE in Tg[CH₄] yr⁻¹; methane radiative forcing, RF in
7 mW m⁻²; methane specific radiative forcing, SRF in mW m⁻² (Tg[CH₄] yr⁻¹)⁻¹. See Sect. 3.2
8 for details.

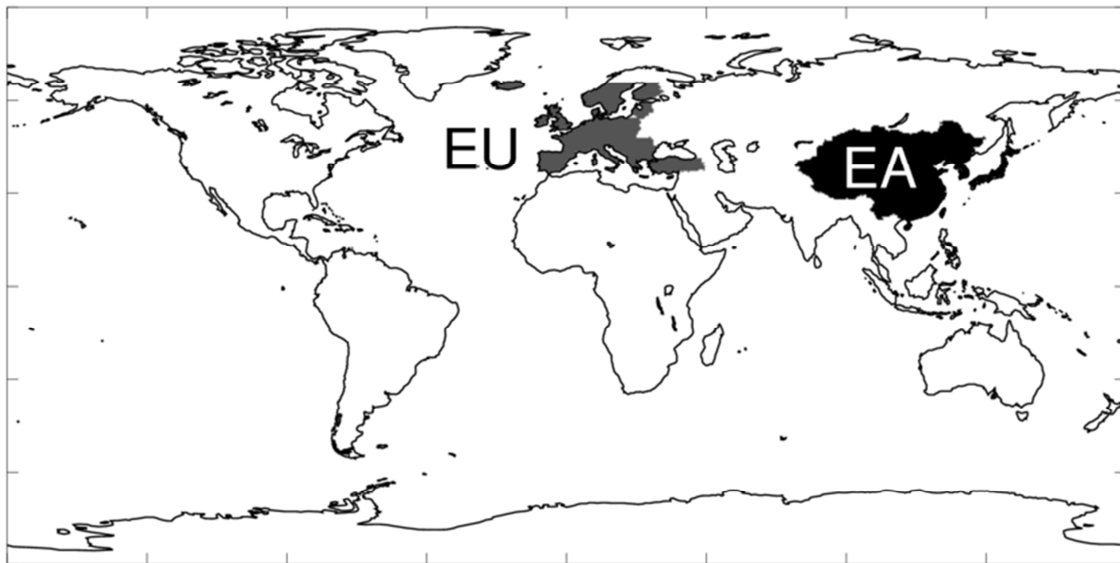
Model	τ_{OH}		τ_{tot}		B		f	ΔE	RF	SRF
	Ctl	Per	Ctl	Per	Ctl	Per				
HadGEM3	6.0	5.6	5.5	5.2	4561	3702	1.34	117	123	1.21
NorESM1	7.8	7.7	7.0	6.9	4815	4489	1.28	36.5	44	1.38
OsloCTM2	10.2	9.6	8.9	8.4	4909	4115	1.46	61	109	2.04

9

1 **7 Figures**

2

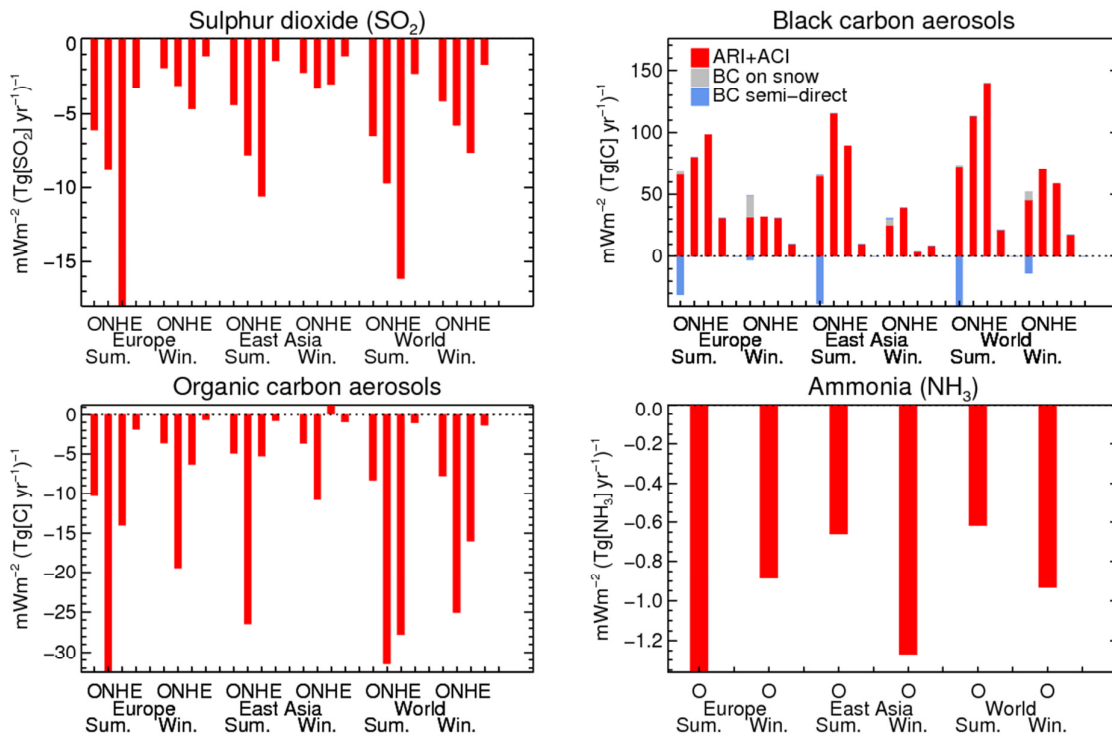
3 **Figure 1.** *HTAP tier-1 regions used in the ECLIPSE specific radiative forcing matrix. EU*
4 *stands for Europe and EA for East Asia.*



5

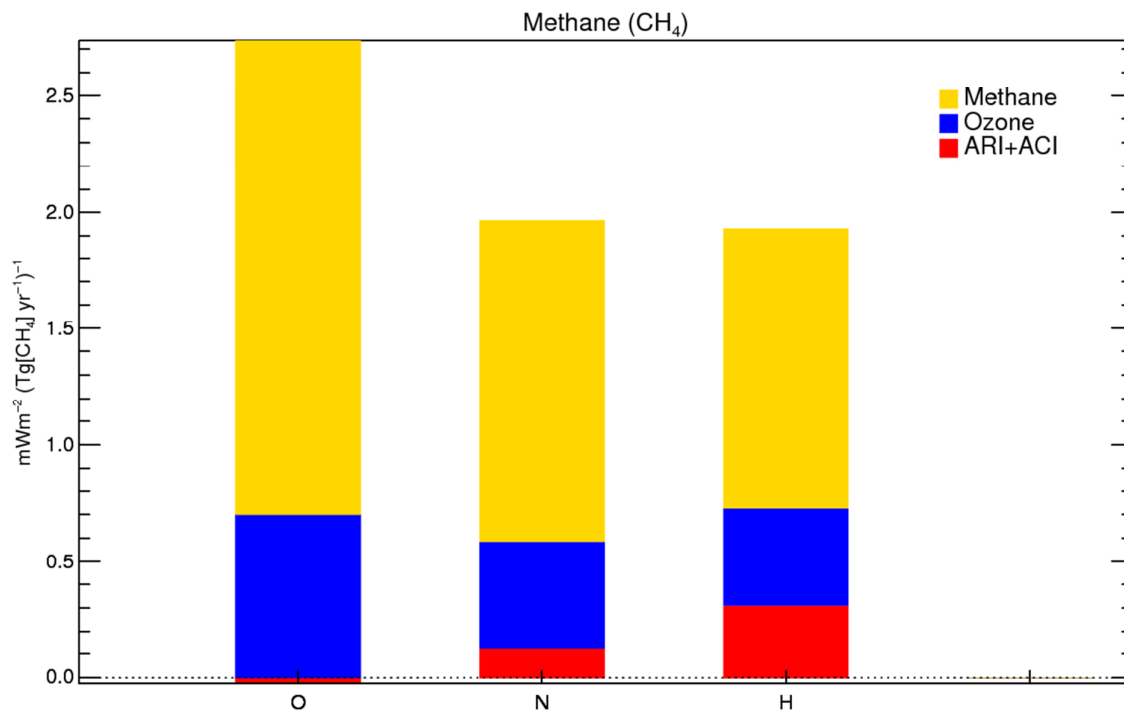
6

1 **Figure 2.** Specific radiative forcing, in $mW m^{-2} (Tg yr^{-1})^{-1}$, for regional and seasonal
 2 reductions in sulphur dioxide, black carbon, organic carbon, and ammonia emissions. Results
 3 are obtained by four global models: OsloCTM2 (O), NorESM1 (N), HadGEM3 (H), and
 4 ECHAM6 (E) except for ammonia perturbations where only OsloCTM2 contributes. Three
 5 categories of radiative forcing mechanisms are included: aerosol-radiation and aerosol-
 6 cloud interactions (red, except for ECHAM6 where aerosol-cloud radiative forcing is not
 7 diagnosed), BC deposition on snow (grey, OsloCTM2 only), and rapid adjustments from the
 8 semi-direct effect of BC (blue, OsloCTM2 only).



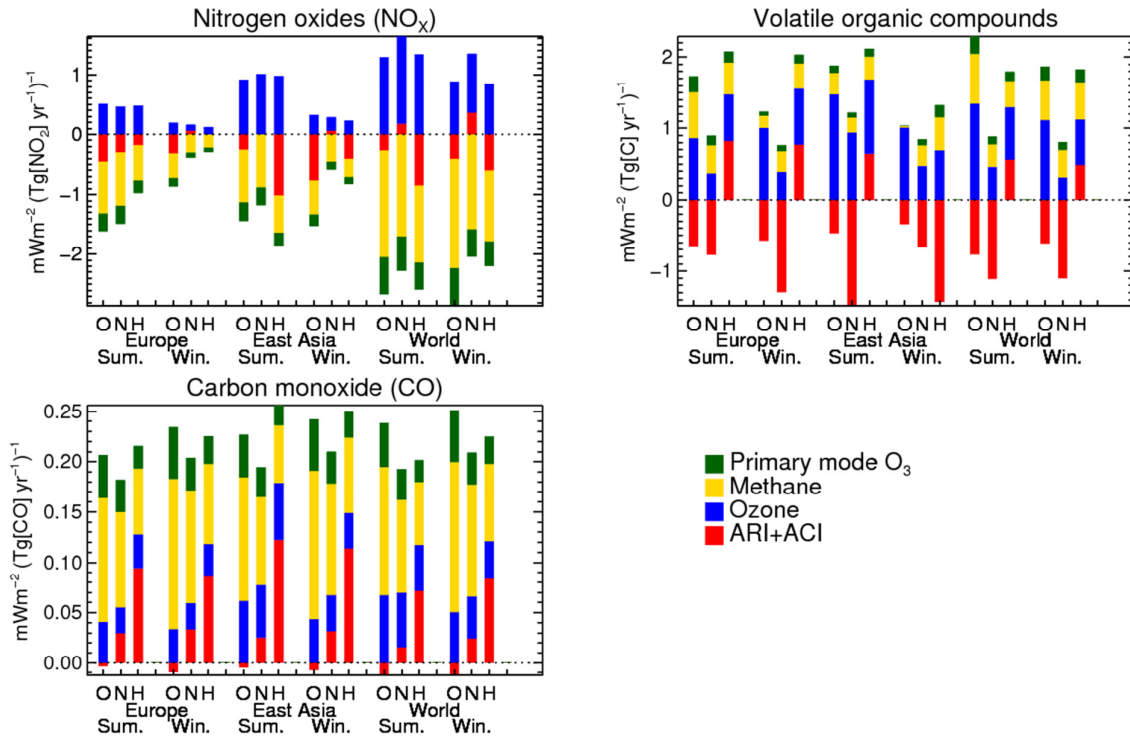
9
10

1 **Figure 3.** Specific radiative forcing, in $mW m^{-2} (Tg[CH_4] yr^{-1})^{-1}$, for global and annual
2 reductions in equivalent methane emissions (see Sect. 3.2 for details). Results are obtained by
3 three global models: OsloCTM2 (O), NorESM1 (N), and HadGEM3 (H). Three categories of
4 radiative forcing mechanisms are included: aerosol-radiation and aerosol-cloud interactions
5 (red), short-term changes in ozone (blue), and methane (yellow).



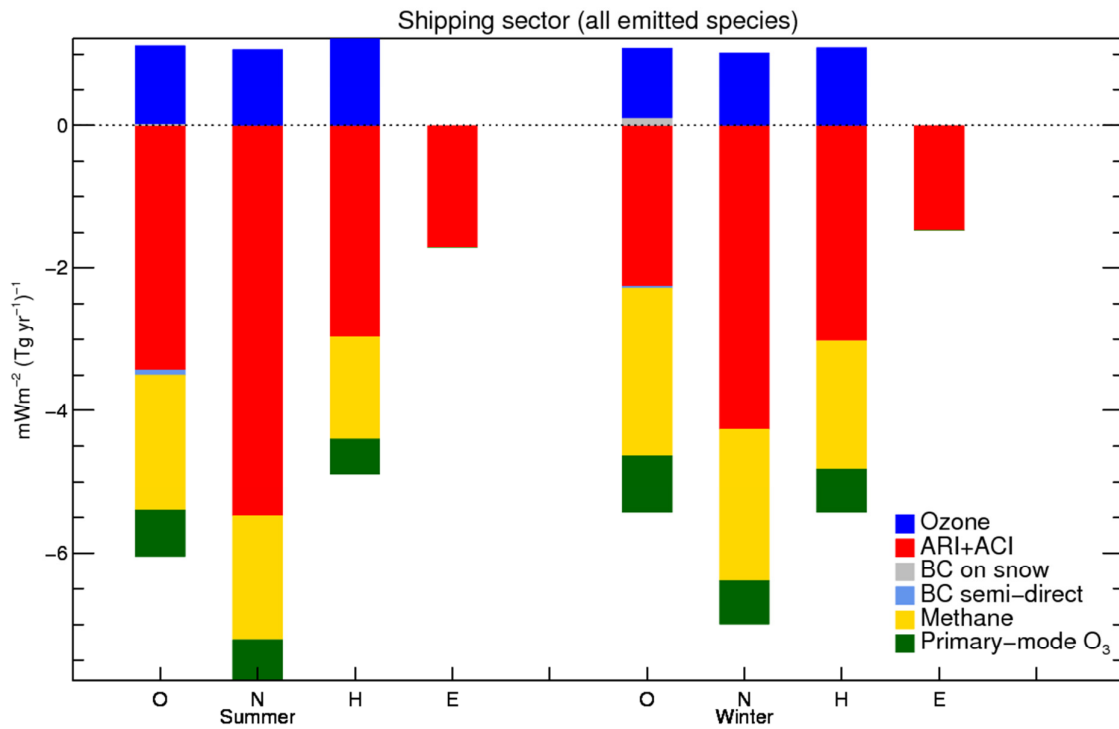
6
7

1 **Figure 4.** Specific radiative forcing, in $mW m^{-2} (Tg yr^{-1})^{-1}$, for regional and seasonal
 2 reductions in nitrogen oxide, volatile organic compounds, and carbon monoxide emissions.
 3 Results are obtained by three global models: OsloCTM2 (O), NorESM1 (N), and HadGEM3
 4 (H). Four categories of radiative forcing mechanisms are included: aerosol-radiation and
 5 aerosol-cloud interactions (red), short-term changes in ozone (blue), methane (yellow), and
 6 primary-mode ozone (green).



7
8

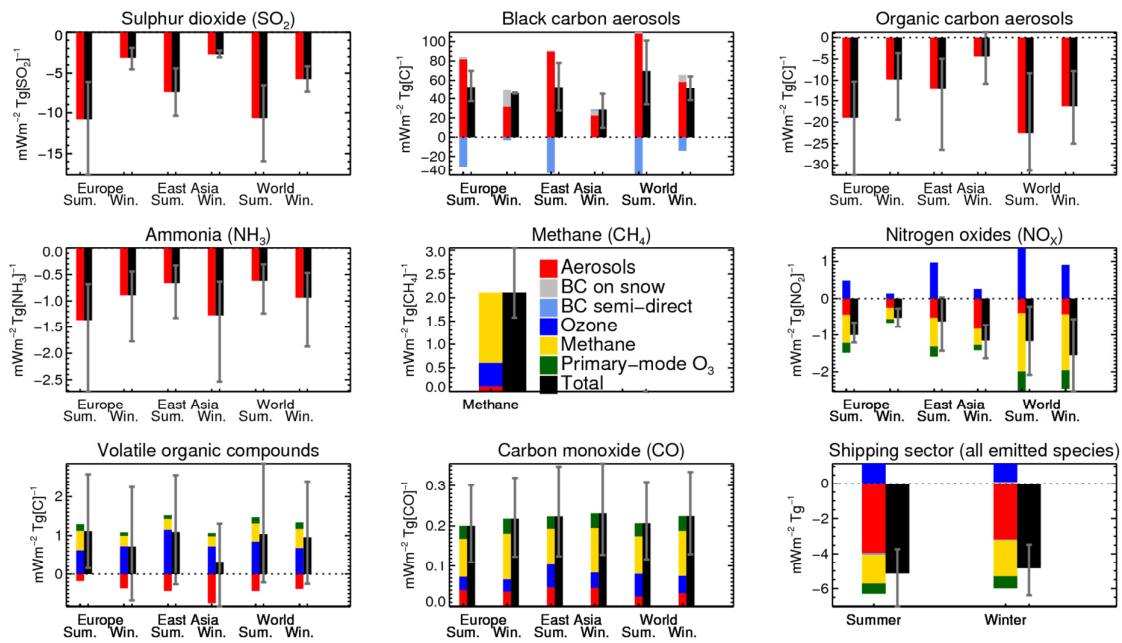
1 **Figure 5.** Specific radiative forcing, in $\text{mW m}^{-2} (\text{Tg yr}^{-1})^{-1}$, for seasonal reductions in all the
 2 species emitted by the shipping sector. The species included and their units of emitted mass
 3 are sulphur dioxide (SO_2), black carbon (C), organic carbon (C), ammonia (NH_3), nitrogen
 4 oxides (NO_2), volatile organic compounds (C), carbon monoxide (CO), and methane (CH_4).
 5 Results are obtained by four global models: OsloCTM2 (O), NorESM1 (N), HadGEM3 (H),
 6 and ECHAM6 (E). Six categories of radiative forcing mechanisms are included: aerosol-
 7 radiation and aerosol-cloud interactions (red, except for ECHAM6 which diagnoses aerosol-
 8 radiation only), black carbon deposition on snow (grey, OsloCTM2 only), black carbon rapid
 9 adjustments from the semi-direct effect (light blue, OsloCTM2 only), short-term changes in
 10 ozone (dark blue, not simulated by ECHAM6), methane (yellow, not simulated by ECHAM6),
 11 and primary-mode ozone (green, not simulated by ECHAM6).



12
13

1

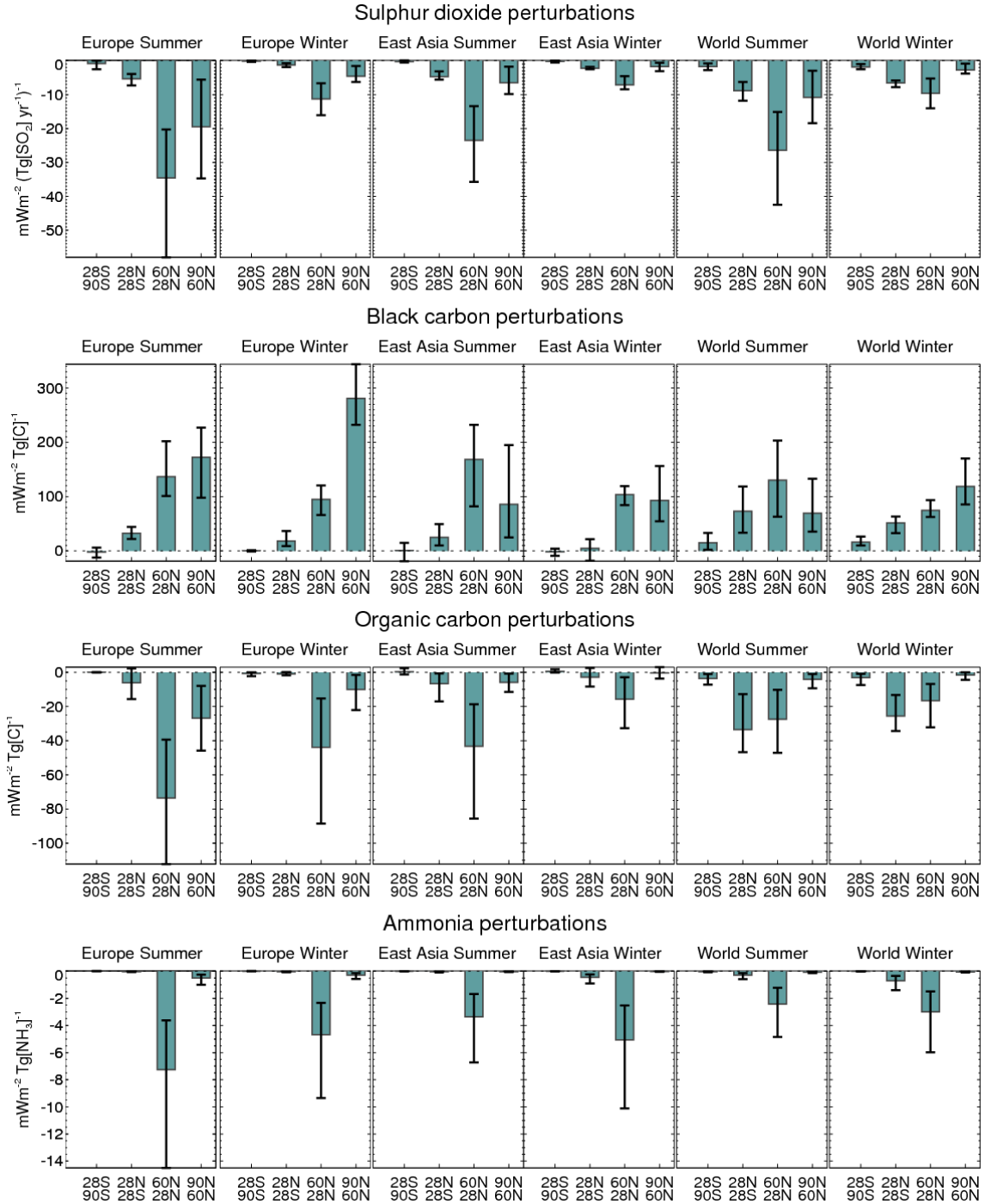
2 **Figure 6.** Best estimates of specific radiative forcing for regional and seasonal reductions in
3 near-term climate forcer emissions, in $mW m^{-2} (Tg yr^{-1})^{-1}$. Best estimates are given for six
4 categories of radiative forcing: aerosol-radiation and aerosol-cloud interactions (red), black
5 carbon deposition on snow (grey), black carbon rapid adjustments from semi-direct effects
6 (light blue), short-term changes in ozone (dark blue), methane (yellow), and primary-mode
7 ozone (green). Black bars show the total specific radiative forcing, i.e. the sum of the six
8 components listed above, and whiskers denote the weakest and strongest specific radiative
9 forcing that are obtained by the four participating models or, in the case of ammonia
10 perturbations, estimated from the literature.



11

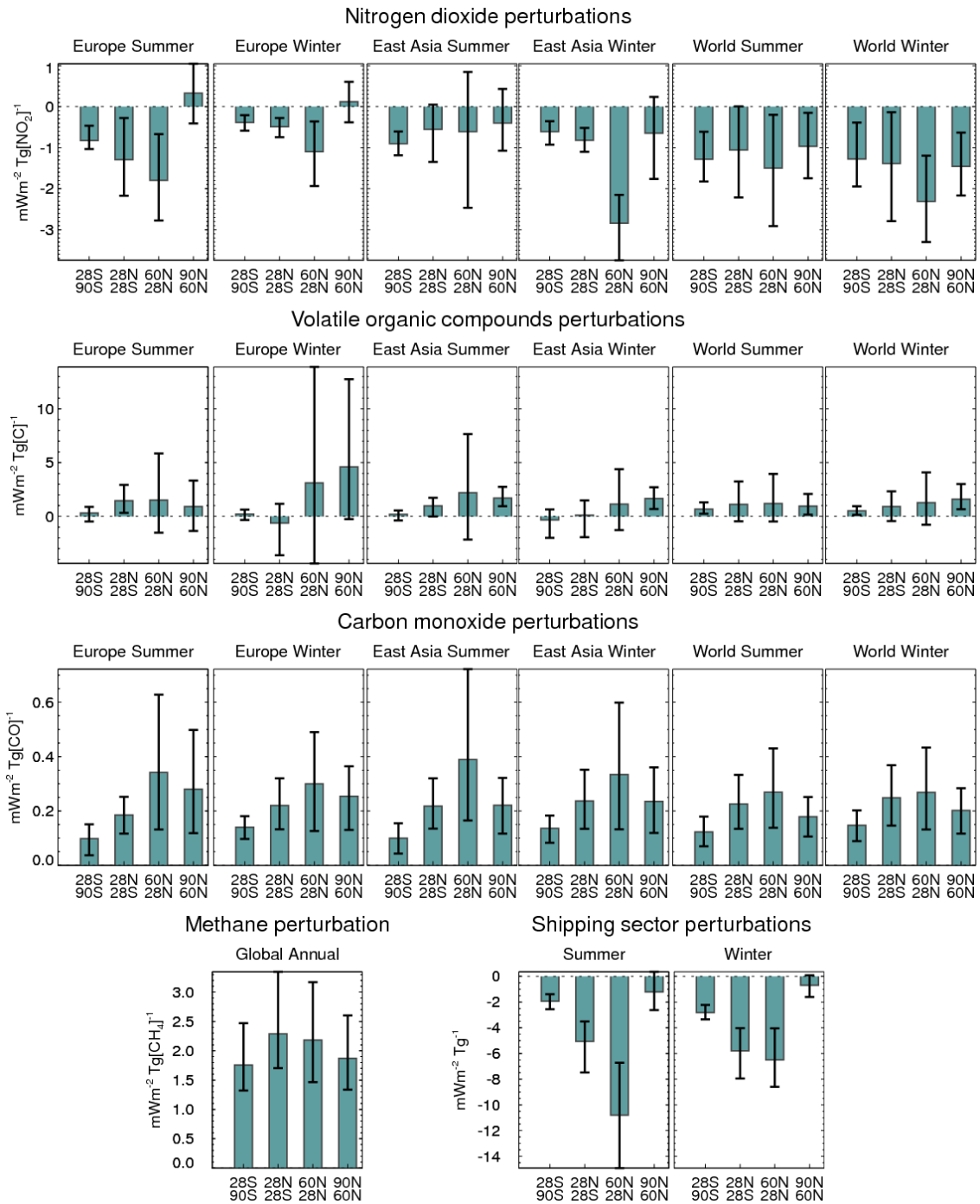
12

1 **Figure 7a.** Best estimates of annually-averaged specific radiative forcing, in mW m^{-2}
 2 $(\text{Tg yr}^{-1})^{-1}$, in four latitude bands, for aerosol primary and precursor emission perturbations.
 3 Each row corresponds to a perturbed species: from top to bottom, sulphur dioxide, black
 4 carbon, organic carbon, and ammonia. Each column corresponds to a regional and seasonal
 5 perturbation. Barcharts are shown for four latitude bands, from left to right: 90N–60N,
 6 60N–28N, 28N–28S, and 28S–90S.
 7



8

1 **Figure 7b.** As Figure 7a, but for ozone precursor and shipping sector perturbations.
 2 Perturbed species are, from top to bottom, nitrogen oxide, volatile organic compounds,
 3 carbon monoxide, methane, and all species emitted by the shipping sector.
 4



5
6